Distribution Agreement

In presenting this thesis or dissertation as a partial fulfillment of the requirements for an advanced degree from Emory University, I hereby grant to Emory University and its agents the non-exclusive license to archive, make accessible, and display my thesis or dissertation in whole or in part in all forms of media, now or hereafter known, including display on the world wide web. I understand that I may select some access restrictions as part of the online submission of this thesis or dissertation. I retain all ownership rights to the copyright of the thesis or dissertation. I also retain the right to use in future works (such as articles or books) all or part of this thesis or dissertation.

Signature:

_____ _____

Yue Ding Date

DNA Supercoiling as a Regulatory Signal for the Lambda Repressor
and
An Integrated Calibration Method for the Molecular Fluorescence Force Probes

Yue Ding
Doctor of Philosophy

Physics

Dr. Laura Finzi
Advisor

Dr. Khalid Salaita
Advisor

Dr. Sergei Urazhdin
Committee Member

Dr. Kurt Warncke
Committee Member

Dr. Eric Weeks
Committee Member

Accepted:

Lisa A. Tedesco, Ph.D.
Dean of the James T. Laney School of Graduate Studies

Date

DNA Supercoiling as a Regulatory Signal for the Lambda Repressor
and
An Integrated Calibration Method for the Molecular Fluorescence Force Probes

By

Yue Ding
B.S., University of Science and Technology of China, 2008

Advisor: Laura Finzi, Ph.D.

Advisor: Khalid Salaita, Ph.D.

An abstract of
A dissertation submitted to the Faculty of the
James T. Laney School of Graduate Studies of Emory University
in partial fulfillment of the requirements for the degree of
Doctor of Philosophy
in Physics
2014

Abstract

DNA Supercoiling as a Regulatory Signal for the Lambda Repressor
and
An Integrated Calibration Method for the Molecular Fluorescence Force Probes

By Yue Ding

In the first part of this dissertation, we studied the role of DNA supercoiling on the stability of the lambda repressor (cI) - mediated regulatory loop. DNA supercoiling senses environmental stress, modifies the accessibility of chromatin, and coordinates the transcription of genes. Therefore, it likely affects protein-mediated long-range DNA interactions, such as looping, which regulate transcription. cI maintains the quiescent stage of bacteriophage lambda in infected *E. coli*, by binding to specific sites and mediating a DNA loop that prevents over-expression of the repressor protein to preserve sensitivity to host conditions that trigger virulence. Here, we assessed how well the cI-mediated DNA loop topologically isolates the cI promoter and determined whether supercoiling enhances cI-mediated DNA looping. We demonstrated that supercoiling levels in cI-mediated DNA loops under conditions of DNA tension and twist were as high as -10 or +16%. Furthermore, supercoiling was essential for DNA looping under tension and lowered the free energy of loop formation by cI. Therefore, the lambda repressor system appears to utilize supercoiling for lysogeny maintenance; it encodes sensitivity to the overall cell health through supercoiling-enhanced looping and creates independent modules of distinct superhelicity.

In the second part of this dissertation, we developed a technique to calibrate fluorescence based probes that are used to measure cellular forces. Despite the importance of mechanotransduction, few methods are available to measure molecular forces in living systems. One of these methods is molecular tension - based fluorescence microscopy (MTFM), a technique that allows visualization of piconewton forces by flanking a flexible polymer by a fluorophore-quencher pair and detecting the fluorescence increase resulting from polymer extension under tension. To accurately calibrate MTFM probes, we integrated a magnetic tweezers system to a total-internal-reflection fluorescence (TIRF) microscope for single molecule fluorescence - force measurement, and designed a 4.4 micron lambda-DNA fragment to link to a surface-immobilized DNA hairpin probe. Preliminary results showed binary fluorescence changes which report on the opening and closing of the hairpin, and its force-extension data, in good agreement with a theoretical model, supporting the idea that this experimental setup could indeed be used to measure molecular forces with high accuracy.

DNA Supercoiling as a Regulatory Signal for the Lambda Repressor
and
An Integrated Calibration Method for the Molecular Fluorescence Force Probes

By

Yue Ding
B.S., University of Science and Technology of China, 2008

Advisor: Laura Finzi, Ph.D.

Advisor: Khalid Salaita, Ph.D.

A dissertation submitted to the Faculty of the
James T. Laney School of Graduate Studies of Emory University
in partial fulfillment of the requirements for the degree of
Doctor of Philosophy
in Physics
2014

Acknowledgement

I would like to express my deepest gratitude and regards to Dr. Laura Finzi and Dr. Khalid Salaita, my dissertation advisors, and Dr. David Dunlap, for their generous support, incomparable guidance, and active participation throughout my PhD years. This dissertation would not be possible without their meticulous suggestions and kind mentorship. It has been a great privilege for me to work with them.

I take this opportunity to acknowledge my sincere appreciation to my committee members, Dr. Sergei Urazhdin, Dr. Kurt Warncke, and Dr. Eric Weeks, for their valuable time, insightful criticism, and constant encouragement on my research. I am also very grateful to other faculty members in the Physics Department, for their thoughtful advice and stimulating discussions.

I am indebted to my former colleagues, Dr. Qing Shao, Dr. Haowei Wang; Dr. Ivan Rasnik, Dr. Kent Lin, and Dr. Julie Coats, for teaching me single molecule techniques and fluorescence microscopy; other members from the Finzi Lab, Dunlap Lab, and Salaita Lab, for their generous help and assistance on research, especially to Dr. Monica Fernandez-Sierra and Dr. Diane Wiener, for their encouragement and support through difficult time during my PhD study.

I owe my utmost appreciation to Dr. David Lynn, my mentor in the ORDER (On Recent Discoveries by Emory Researchers) program, for encouraging my passion for sharing science with general audiences, providing me with this great opportunity, and seeing the teacher in me before I did. Further thanks go to my colleagues in the program, for creating an incredible experience in collaborating and teaching our own research while developing methodology and practical skills in undergraduate education.

My profound gratitude and reverence goes to my parents, Mr. Yongning Ding and Ms. Xiaoli Huang, and my late grandparents, Mr. Jida Ding and Ms. Shuirong Zhao, for their deepest love, unconditional support, and longtime sacrifice they made in bringing me up and helping me become a better person. I would like to honor them with my work.

I would like to thank my dearest friends, especially to Xinxian Shao, Dr. Yuan Zhou, and Ling Ling, for their warmest friendship, company, and inspiration. It is my great fortune to grow with them.

I received help and assistance in numerous occasions from members in the Physics Department, the Laney Graduate School, and other members of the Emory community. I have my deepest gratefulness and apologies for not being able to mention all their names. This dissertation is dedicated to all of them.

Table of Contents

List of Tables and Figures

Part I: DNA supercoiling: A Regulatory Signal for the Lambda Repressor

Part II: A Combined Magnetic Tweezers (MT) and Single Molecule Fluorescence Resonance Efficiency Transfer (smFRET) Instrument to Calibrate Molecular Tension - Based Fluorescence Probes

Part I: DNA supercoiling:

A Regulatory Signal for the Lambda Repressor

Chapter 1 Introduction

1.1 DNA Supercoiling: A common DNA feature

Supercoiling is one of the most common features of DNA topology. In physiological conditions, the two single strands of the DNA molecule naturally wind around each other once every 10.4-10.5 base pairs, forming the right-handed, double helical conformation known as "relaxed B-form DNA." *In vivo*, the activity of motor proteins or enzymes such as topoisomerases, helicases or polymerases may introduce torsional strain into a given segment of double-stranded DNA that is topologically constrained at both ends. In this case, the twist of the DNA molecule may change. This means that the pitch of the double helix may increase in the case of overwinding or decrease in the case of underwinding. Past a critical threshold, the axis of the double helix will collapse and cross itself at one or more points forming loops, buckles, writhe, or (in less rigorous terminology) supercoils. Positive supercoiling results from overwinding DNA while negative supercoiling results from underwinding DNA. DNA will adopt the topology that maintains the lowest free energy (1). DNA supercoils are also called "plectonemes", supercoiled DNA, or plectonemic DNA.

In topologically constrained DNA, the sum of twist (*Tw*) and writhe (*Wr*) is a constant, called the linking number, *Lk*, of this DNA segment (Figure 1.1). The number of right-handed helical turns in a stretch of relaxed B-DNA (length in bp/10.4 base pairs per turn) is defined as the basic linking number, Lk_0. When torsion is introduced, the change in linking number, $\Delta Lk = Lk - Lk_0$, is the number of turns added to or subtracted from the

relaxed state. The supercoiling level for this DNA segment, or "superhelical density" σ, represents the change in linking number relative to the basic linking number: $\sigma = \Delta Lk / Lk_0$.

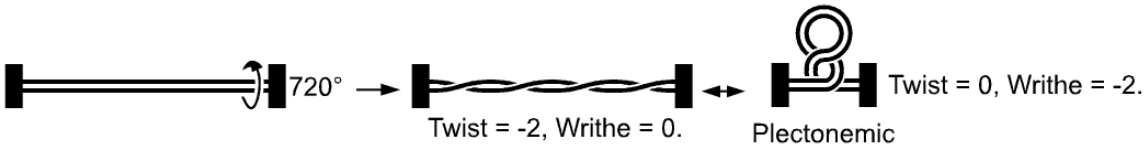

Figure 1.1. DNA supercoiling topology. This is an example of the transition between twist and writhe after adding -2 linking number (negative supercoiling) to a topologically constrained linear DNA (modified from http://en.wikipedia.org/wiki/File:Linear_DNA_Supercoiling.png).

1.2 The importance of supercoiling: A messenger in gene regulation

In most organisms, DNA is negatively supercoiled. The average supercoiling level in eukaryotes is around -6%. This level is constantly and actively regulated by motor proteins including polymerases and topoisomerases, and has been known to affect protein-DNA interactions as it induces structural changes of DNA. Supercoiling affects most of the DNA-related cellular signaling processes, from DNA packaging, replication, and transcription, to DNA repair and recombination.

DNA supercoiling is a mechanism of transcriptional regulation that functions by promoting local melting of base pairs, inhibiting transcription elongation, uncoupling the process of transcription and translation, enhancing promoter function, or coupling with

several promoters (2-9). Sensing environmental changes (pH, concentration of ATP, etc) and subsequently affects genetic regulatory networks, supercoiling serves as a second messenger in gene regulation in cases like transcription of oncogenes (8) or virulent gene infection (7, 9).

1.3 Lambda repressor-mediated loop and other protein-mediated DNA loops

The lambda bacteriophage loop is a model genetic switch that determines the lytic *vs*. lysogenic growth mode of bacteriophage lambda (10-12). The loop is mediated by the lambda repressor, or cI protein, which binds to a pair of tripartite recognition sites (operators) along the DNA, *oL* and *oR*, and forms a 2317-bp loop through cooperative protein-protein interaction (10). Transcription of the lytic genes is suppressed and the bacteriophage lambda maintains its quiescent state, until environmental stress, such as UV radiation, or host *E. coli* starvation, promotes the rupture of the cI-mediated loop, which commits the phage to virulence (Figure 1.2). The role of supercoiling as a second messenger for sensing environmental changes suggests that it may also play a role in this regulatory protein-mediated loop, and that the lambda repressor-mediated DNA loop may be sensitive to the level of supercoiling of the genome in which in which it is embedded.

The hierarchical structural state of metaphase chromatin *in vivo* is comprised of coils and loops, and during interphase chromatin loops are known to control the regulation of certain functionally group related genes. In eukaryotes, chromatin conformation capture (3C) experiments revealed loops of hundreds of kilobases or even megabases throughout

different genomes (13, 14). Recent experiments showed that not only do such structural domains coincide with transcriptional boundaries, but also that transcriptional activity effectively remodels these domains and alters supercoiling of the DNA (15). Transcription also alters supercoiling in prokaryotes (16), in which there was evidence for some 400-500 dynamic loop domains ranging from 2 to 66 kbp in size (17). Recent observations by super-resolution microscopy in live bacteria and 3C assay analysis (18) found that H-NS, a global transcription silencer and one of the nucleoid-associated proteins (NAPs, proteins that arrange dynamic spatial organization of chromosomes), may form ~2 compact clusters per chromosome to anchor the crosslinkings between tens of different domains and organize 3D architecture in *E. coli* chromosome, driven by its DNA-bound oligomerization.

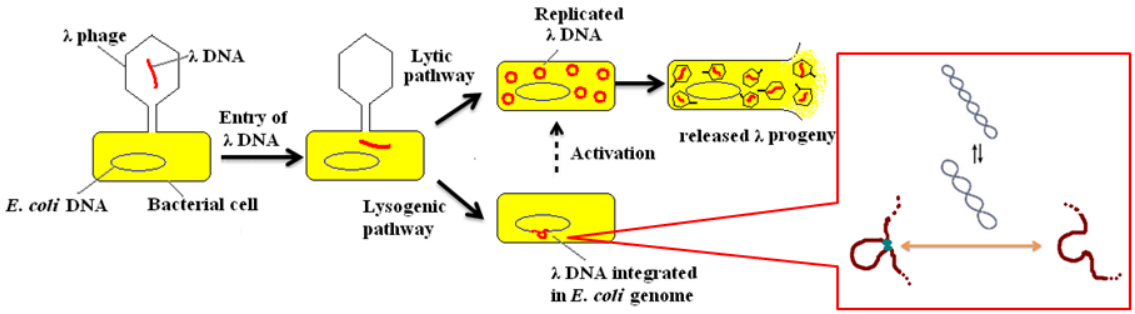

Figure 1.2. The genetic switch in bacteriophage lambda pathways. Schematic representation of the lambda bacteriophage infection of the bacterium *E. coli* highlights the two possible outcomes of infection (i.e. lysogenic and lytic pathways), and the fact that both the loop and supercoiling effect on the lambda switch.

A plasmid is a circular piece of DNA that can replicate independently of chromosomal DNA within a cell. Simultaneous binding of soluble proteins with high affinity for two sets of binding sites, which are widely separated along the plasmid contour, creates two distinct topological domains. Previously published experiments have shown that simultaneous LacI binding to synthetic tandem sequences of lac repressor binding sites can divide a plasmid into separate topological domains with different supercoiling levels (19). In those experiments, supercoils constrained in a 2.9 kbp LacI-mediated topological domain were released into the other domain through the protein closure as slowly as 0.0062 supercoils/min. Apparently, those loops were much larger than the 100-400 bp loops usually created in *E. coli* by LacI.

Since the LacI tetramer might have evolved not only to secure loops, but also to overcome the resistance to bending the DNA into small loops (90 to 400 bp-long), new experiments were conducted with the bacteriophage lambda repressor (cI) which secures a 2317 bp loop in the phage DNA through specific binding to a pair of tripartite recognition sites (operators). The cI-mediated loop has no appreciable bending strain, but the free energy equivalent of the entropic penalty associated with forming such a long loop is significant at 10.2 kcal/mol under room temperature (11, 20). Recent work indicated that loop closure by cI may be mediated by oligomers involving not only specifically bound, but also non-specifically bound protein (10-12). To probe how good of a barrier to torsional relaxation the cI repressor closure is, experiments were conducted by our collaborators (Ding et al., under revision; please see Appendix 1) using plasmids with operators separated by 2317 or 1051 bp. Rates were measured at which supercoils,

originally trapped in one domain of a plasmid, crossed a cI junction and dissipated in the other nicked, torsionally unconstrained domain. These experiments probed the stability of cI junctions against biochemically accessible levels of supercoiling, and showed that the longer the nicked segment, the shorter time it takes for supercoils to dissipate through the junction. To access arbitrary, higher levels of torsion, linear DNA segments with these operators were twisted with magnetic tweezers by ±10%, and the superhelical density captured in spontaneous cI-mediated loops was measured. Fitting results from the extension *versus* twist curves of our experiments suggest that unlooped DNA forms plectonemes with wider gyres than looped DNA; thus the loop may nucleate a more tightly-wrapped plectoneme.

While these experiments probed whether cI-mediated loops constituted torsional barriers, supercoiling has also been shown to affect the probability of loop formation (21). If looping were sensitive to discrete levels of supercoiling, it would imply that superhelical density can act as a general regulatory signal for transcriptional events, as has been shown for transcriptional repression by the Gal repressor (2, 3). To quantitatively investigate cI-mediated looping as a function of superhelical density, looped/unlooped equilibria were measured in DNA tethers with different levels of DNA supercoiling level. We found that a threshold level of negative supercoiling was essential for looping in DNA under slight tension. In addition, increased supercoiling compensated for increased tension.

1.4 Magnetic tweezers (MT): The ideal method to stretch and twist polymers

The early 1990s witnessed the emergence of single molecule force manipulation techniques and a new era for investigating polymer properties under tension and/or torsion. The common characteristic for these techniques including optical trap (OT) (22), magnetic tweezers (MT) (23), and atomic force microscopy (AFM) (24), is that they all require surface immobilization for the observation and manipulation of a single molecule. Among them, MT have the unique advantages, including straightforward control of the supercoiled state of DNA, easy integration with fluorescence measurements, and simple, robust experimental configuration (25).

As stated above, a typical MT experimental configuration is simple (Figure 1.3, left): A strand of polymer (usually DNA or RNA) is tethered in a flow chamber between a glass surface and a paramagnetic bead, usually by a noncovalent bond that can resist forces on the order of a hundred piconewton magnitude (26-30). A pair of permanent magnets is suspended above the chamber that applies a magnetic field to the chamber. The upward stretching force $\mathcal{F}$ exerted by the magnetic field on the bead is given by:

$$\mathcal{F} = \tfrac{1}{2}\nabla(\mathcal{m} \cdot \mathcal{B}), \qquad \text{(Eq. 1)}$$

where $\mathcal{m}$ is the induced magnetic moment of the bead in an external magnetic field, $\mathcal{B}$. Due to the much smaller size of the tethered bead (~μm) compared to the length scale over which the magnetic field (~mm) may change, the force $\mathcal{F}$ experienced by the bead (and the tethering polymer) is constant at a fixed magnet position, and can be easily

varied by changing the distance between the magnets and the chamber, usually between ~10 fN to ~100 pN. The range of force of interest in studies on protein-mediated DNA looping is between 0.1 pN to 1 pN, since higher forces tend to abrogate the thermal fluctuations that lead to long-range molecular interactions. Twisting of the DNA is achieved by rotating the pair of magnets.

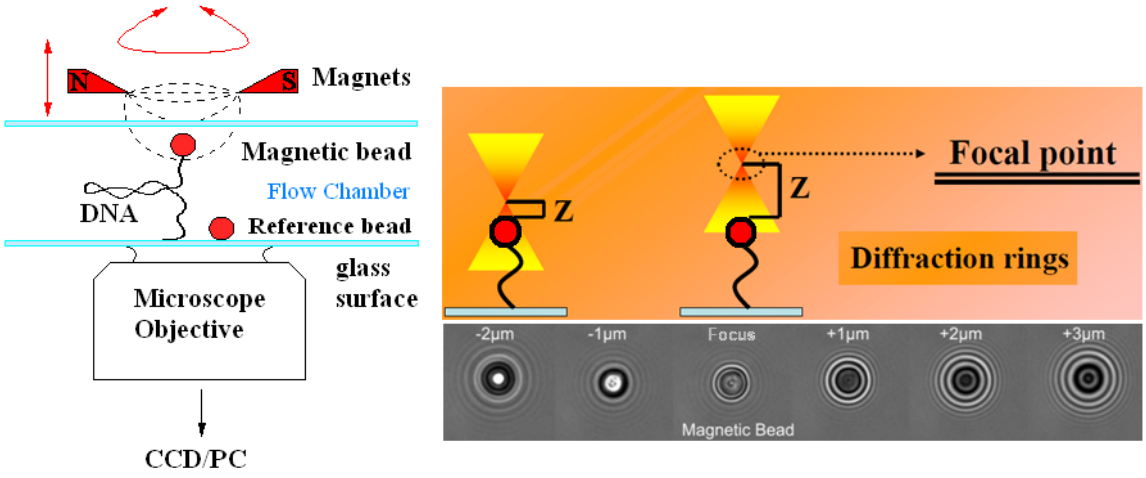

Figure 1.3. General design of magnetic tweezers. (Left) A simplified schematic representation of the magnetic tweezers setup with the DNA tether and a "reference bead" stuck on the surface inside a glass flow chamber. The attachment between the DNA and the bead/glass surface (not shown) is usually achieved by taking advantage of the specific interactions between biotin and streptavidin, and between anti-digoxigenin and digoxigenin. One end of the DNA is labeled with multiple biotin, while the other end is labeled with multiple digoxigenin. The glass surface can then be coated with streptavidin and the bead with anti-digoxigenin, or vice versa. (Right) Distinctive diffraction ring patterns of the DNA-tethered bead are used for DNA extension measurement by comparing a stack of them with that of the stuck bead ("reference bead").

The equipartition theorem is typically applied to determine the force $\mathcal{F}$ applied on the tether in experiments. The energy of one degree of freedom is

$$E_p = \frac{1}{2}k_BT; \quad \text{(Eq. 2)}$$

Considering the DNA tether - bead system similar to a vertical pendulum,

$$E_p = \frac{1}{2}\mathcal{F}\langle\delta x^2\rangle/l, \quad \text{(Eq. 3)}$$

Thus, by measuring the extension of the molecule l and the variance of the bead excursions $\langle\delta x^2\rangle$, one can calculate the force

$$\mathcal{F} = k_BTl/\langle\delta x^2\rangle. \quad \text{(Eq. 4)}$$

The variance of the bead excursions can be measured by tracking the motion of the center of the bead in the (x, y) plane, and the tether extension can be measured by generating a z stack of the diffraction ring patterns of the tethered bead above its focal plane and comparing them with the diffraction ring patterns of a stuck bead on the surface ("reference bead") (Figure 1.3, right) (25).

1.5 DNA behavior under torsion and tension: Hat curves and force-extension curve

In vivo, DNA is thought to be most often under certain level of tension as well as torsion because of the physiological processes it undergoes. Besides the torsion-inducing enzymes reviewed in section 1.1, DNA is under piconewton-range tension when packaged into bacteriophage capsids, replicated, or transcribed (31-34).

Magnetic tweezers may be used to stretch as well as twist DNA (35). A typical extension *versus* rotation curve for the DNA depends on the magnitude of force applied (Figure 1.4, left): under low force (<1 pN), positive or negative supercoils form when the DNA is wound or unwound, respectively, and the formation of plectoneme (DNA supercoiling cluster) decreases the DNA extension. The extension vs. rotation curve has the shape of a hat and thus is called a "hat curve". Under higher force (1~8 pN), since B-form DNA is right-handed, positively supercoiled DNA behave in the same way as described above, while negatively supercoiled (unwound) DNA denatures more and buckles less with increasing force (36, 37); the extension vs. rotation curve then becomes asymmetric. Several theories have been developed to analyze extension vs. rotation curves under different forces using an elastic rod model (38-41). Of these, the better developed was published by J. Marko in 2007 based on a minimization of the free energy approach (40). He characterized the behaviors of DNA with a few key properties of DNA elasticity, including the persistence length (bending rigidity, characterizing the stiffness of the DNA molecule) (42) and the torsional persistence length (torsional rigidity) (43) of DNA. The DNA elasticity properties represent internal property of the DNA but are also expected to change depending on the buffer condition, especially ionic strength and magnesium concentration. Typically, the persistence length for B-form DNA is around 50 nm under physiological conditions (~10-100 mM monovalent salt) (44). More details about DNA elastic properties are provided in section 4.2.

Similar curves on different DNA fragments were reported previously in the literature (35, 42, 45-47). Several models have been used to classify the DNA extension response to

force (Figure 1.4, right). The worm-like chain (WLC) model (usually for forces ~5-10 pN) developed by J. Marko and E. D. Siggia in 1995 (42), and its later improvements considering elastic stretching terms (for forces >5-10 pN) (46) are most commonly applied.

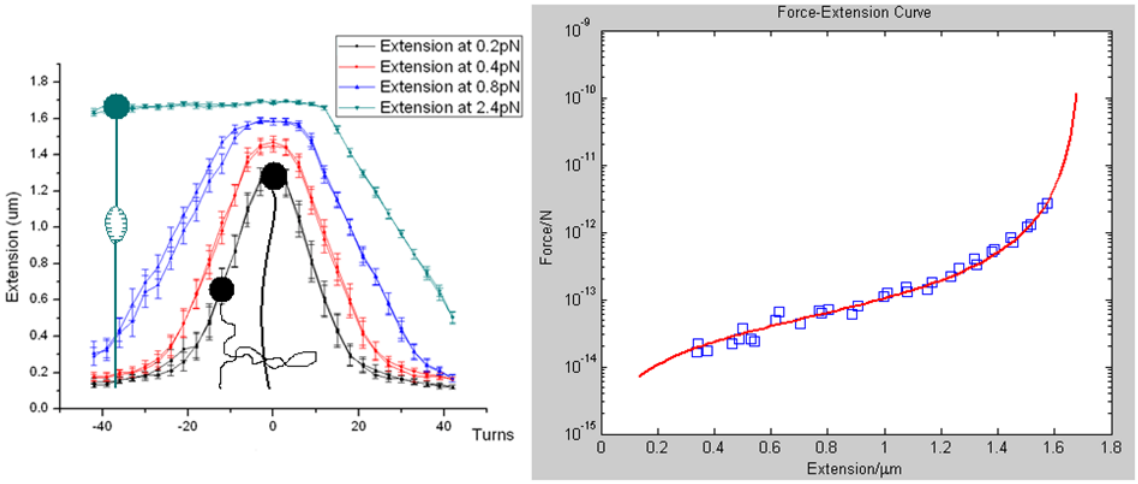

Figure 1.4. DNA hat curves and force *versus* extension curve. (Left) Extension *versus* rotation curve for a 5kbp DNA tether (construct design described in section 3.1) under different force conditions, with diagram schematics of DNA states consistent with particular conditions of tension and torsion. The data points were acquired by following procedures described in section 3.2 and 3.3. (Right) The force *versus* extension curve for the same 5 kbp DNA tether. Blue square: experimental data. Red curve: the worm-like-chain (WLC) model fitting of the experimental data. The extrapolation of the WLC fitting gives the expected full contour length of the DNA.

The WLC model relates the force applied on the DNA molecule $\mathcal{F}$ to the extension of the DNA (end-to-end distance) z, the DNA contour length L, and the persistence length (P). As mentioned above, P is a measure of how stiff the molecule is: the bigger P is the stiffer is the molecule:

$$\mathcal{F} = \frac{k_B T}{P}\left[\frac{1}{4(1-\frac{z}{L})^2} - \frac{1}{4} + \frac{z}{L}\right] \quad \text{[Eq. 5]}$$

In the second part of this dissertation (section 7.5, section 8.2), the force - extension curve will be measured and its WLC fitting will be carried out to calibrate a magnetic tweezers setup that I integrated to a commercial fluorescence microscope.

1.6 Research questions

The questions addressed in this dissertation are focused on the dynamics of the cI-mediated DNA loop in conditions of DNA tension and torsion which mimick those that DNA could experience *in vivo*. In particular, we were interested in 1) whether or not long-range interactions mediated by soluble or membrane-bound proteins that secure DNA loops can block supercoil diffusion and maintain torsional differences between two adjacent loops of chromatin, and 2) whether supercoiling favors the formation of loops. The cI protein from the lambda bacteriophage is an ideal model system to address these questions because of 1) the fact that a wealth of biochemical data are available on this protein and its binding to individual sites on DNA, and 2) the experience that the Finzi group has matured with this particular protein.

Chapter 2 Materials and Methods

2.1 Design of plasmid DNA constructs for supercoiling study in MT experiments

DNA constructs for magnetic tweezers (MT) experiments in the study of the effect of supercoiling on protein-induced DNA looping were formed by tethers of either 4.4kbp or 4.95 kbp containing the λ oL and oR regulatory regions ligated at both ends to a biotin-labeled fragment and a digoxigenin-labeled fragment, respectively, using T4 DNA ligase (New England Biolabs, NEB). Tether segments with four different separations between the oL3 and oR3 sites (loop lengths) bp were produced as indicated in Table 2.1. Biotin- or digoxigenin-labeled end fragments of 800 -1000 bp were created using PCR (KOD Hot Start Polymerase kit, Novagen) with the primer pairs and templates listed in Table 2.2 and Table 2.3 to incorporate about 5%~10% biotin or digoxigenin-labeled dUTP. Appropriate double digestions (listed in Table 2.2) were used to generate complementary ends for ligation to the central DNA fragments. All restriction enzymes were from NEB.

The DNA constructs were attached at one end to the anti-digoxigenin-coated glass surface of a flow chamber and at the other end to a 1.0 μm-diameter streptavidin-coated, paramagnetic bead (Dynabead MyOne Streptavidin T1, Invitrogen, Carlsbad, CA). Multiple biotin-streptavidin bonds at the bead surface and digoxigenin-anti-digoxigenin bonds at the glass surface torsionally constrained the tethers. Flow-chambers of ~ 50 μl volume were assembled between two glass coverslips spaced by double-sided scotch tape and lined with silicon grease. DNA tethers were incubated for at least one hour in λ buffer (10 mM Tris-HCl (pH 7.4), 0.1 mM ethylenediaminetetraacetic acid (EDTA), 200

mM KCl, 0.2 mM dithiothreitol (DTT), 5% dimethyl sulfoxide (DMSO), and 0.2 mg/ml α-casein).

Tether length (bp)	Loop size (bp)	Template or input DNA	DNA production method	Primers/Restriction enzymes
4397	393	pDL944	PCR	NAR & NHE/NarI & NheI
4948	1051	pDL1051	mini prep	--/NgOMIV & DraIII-HF
4959	1231	pDL955A	mini prep	--/HindIII & NgOMIV
4983	1662	pDL950B	mini prep	--/NcoI & DraIII-HF

Table 2.1. Tether fragments for MT experiments. Linear DNA segments were produced either by PCR amplification from a plasmid template or direct digestion of the plasmids. Restriction enzymes were then used to generate "sticky" ends for ligation to biotin- or digoxigenin-labeled attachment fragments (Table 2.2).

Amplicon	Labeled Nucleotide	Plasmid template	Forward Primer	Reverse Primer	Restriction Site
393-biotail	bio-dUTP	pDL944	λbiotailF	λbiotailR	NarI
393-digtail	dig-dUTP		λdigtailF	λdigtailR	NheI
1051-biotail	bio-dUTP	pDL1051	S/pDL2317/2526	A/pDL2317/3645	DraIII-HF
1051-digtail	dig-dUTP		S/pUC19/2019	A/208-12/337	NgOMIV
1231-biotail	bio-dUTP	pDL955A	S/pDL2317/2526	A/pDL2317/3645	NgOMIV
1231-digtail	dig-dUTP		S/pUC19/2019	dig-control	HindIII
1662-biotail	bio-dUTP	pDL950B	S/pDL2317/2526	A/pDL2317/3645	NcoI
1662-digtail	dig-dUTP		S/pDL2317/2526	A/pDL2317/3645	DraIII-HF

Table 2.2. PCR reagents for attachment fragments. Biotin- and digoxigenin-labeled DNA fragments about 1000 bp in length were produced and ligated to opposite ends of the tether fragments in order to attach opposite ends of the tethers to the anti-dig-coated glass and the streptavidin-coated, paramagnetic beads. After PCR to produce the desired fragment with the indicated labeled nucleotide, "sticky" ends complementary to those of the tether fragments were generated by restriction digest.

Primer Name	**DNA Sequence (5' to 3')**
NAR	TCCAGAGGCGCCCTCACCGGCTCCAGATTTATCAGCAATAAAC CAGCCAGCCGGAAGGGCCGAGCGC
NHE	TGGTAAGCTAGCCTGGGGCCAGATGGTAAGCCCTCCCGTATCGT AGTTATCTACACGACGGGGAGTCAGG
λbiotailR	CTGCGCACAAACCATAGATTGC
λbiotailF	CTGCCTCTTTCTCTTCACGG
λdigtailR	CTGGCCCTGCTTATTACAGGATGTGCTCAACAGACGTTTACTGT TCAAAACAAACCG
λdigtailF	CTGATAACGGACGTCAGAAAACCAGAAATCATGGTTATGACGT CATTGTAGGCGGAGAGC
S/pDL2317/2526	TGTATGGAACAACGCATAAC
S/pDL2317/3645	TCCAAACTGGAACAACAC
A/208-12/337	TGGCGTAATAGCGAAGAG
S/pUC19/2019	TGCACAACATGGGGGATCAT
dig-control	GACTGATAGTGACCTGTTCGTTGCAACAAATTGATAAGCAATGC
S/pUC19/2412	TGGGTGAGCAAAAACAGGAAGGCA
A/pUC19/1435	CGTAATCTGCTGCTTGCAA

Table 2.3. DNA sequences of PCR primers.

2.2 DNA manipulation for supercoiling studies

For a normal single molecule magnetic tweezers experiments without fluorescence, DNA was stretched and twisted using a pair of permanent magnets on a mount above the microscope stage which could be both translated along, and rotated about, the optical axis of the microscope. Details regarding the microscope can be found in previous publications (48). First, torsionally constrained DNA tethers were identified by twisting them to verify that plectonemes formation would reduce the overall extension. Under both low and high forces (0.2 and 3 pN, respectively) the tethers were unwound to $\sigma \sim -10\%$ (-42 turns for ~ 4950 bp DNA), rewound to +10%, unwound to -10% again, and unwound back to 0 in steps of 3 turns while recording the extension. This produced overlapping extension versus twist curves. These curves are symmetric at low tension under which plectonemes form and there are no phase transitions to denatured or left handed helices (49). Under high tension (~ 3 pN), the peaks of such curves indicate the contour lengths of torsionally relaxed DNA. Then tethers were gently stretched and twisted both before and after the addition of cI protein diluted in λ buffer to a final concentration of 160 nM (393 bp loops) or 200 nM (all other loops). Wild-type cI protein from the laboratory of Sankar Adhya (NIH) was used for experiments with 393 bp loops, and a His-tagged protein provided by Keith Shearwin (University of Adelaide) was used with all other loops. Wild-type and His-tagged cI proteins behave identically in looping experiments *in vitro* (50). Two types of experiments were performed. In one, the tether extension was recorded at constant tensions between 0.1 ~ 0.8 pN to detect the DNA supercoiling level (σ) constrained in lambda repressor-mediated loops that formed spontaneously in extensively twisted DNA. In another, extension was recorded as a

function of time under constant tensions at different levels of σ to monitor spontaneous loop formation and breakdown.

2.3 Data acquisition and analysis for supercoiling study: The change-point algorithm

Using video-rate, three-dimensional tracking, *X*, *Y*, and *Z* coordinates of mobile (tethered) and non-specifically stuck beads were acquired at 10 frames/s. From the extension of the tether along the microscope axis and the transverse excursions of the tethered bead perpendicular to the direction of the magnetic field, the tension in the molecule was determined using the equipartition theorem. The time versus extension data was then analyzed to identify probable looping events. A Matlab-coded "change-point" algorithm and expectation-maximization routine (51, 52) was used to parse the time series for looped and unlooped states without filtering or averaging which requires assumptions on structural states. The looped (τ_L) and unlooped (τ_U) lifetimes and the associated uncertainties were determined by optimization of the maximum likelihood function for the lifetime segments and fitting with an exponential distribution with at least 150 data points. The energy associated with looping under various tension and twist conditions was calculated using $\Delta G/kT = - ln (\tau_L / \tau_U)$. Error bars were 99% confidence intervals for mean lifetimes determined from the exponential fit or the propagation of errors from lifetime measurements in the calculation of looping energies.

Chapter 3 Results and Discussion

3.1. cI-loops can constrain high levels of supercoiling

To examine whether or not more torsional energy can be confined within a loop secured by lambda repressor, the DNA supercoiling level (σ, the change in linking number in a DNA molecule divided by the linking number of the same molecule in its relaxed state; see section 1.1) was varied in the range of ±10% using the tweezers (23) to twist DNA tethers in the absence or presence of cI protein. In the absence of protein, when the torque surpassed a critical level in the tether, the DNA buckled and formed plectonemes which reduced the extension of the tether (Figure 3.1, black curve). At higher tension the curves were not symmetric as expected, since while overwinding still produced B-form plectonemes, unwinding induced a phase change without significant length reduction (49, 53). Under moderate tension, less than 0.5 pN, either under- or over-twisting produces similar plectonemes of B-form DNA and a symmetric extension *versus* twist curve.

When DNA was twisted under moderate tension in the presence of cI, plectonemes formed as usual, but when highly plectonemic molecules were unwound, extension versus rotation curves were often shifted and/or exhibited maxima reduced by a length comparable to the loop length (Figure 3.1, red and blue curves *vs.* black curve). The shift indicated the amount of twist that had become constrained within a DNA loop that formed in an extensively plectonemic molecule, which no longer influenced the extension of the remainder of the DNA tether outside the loop. cI-mediated loops were expected to reduce the maximum extension, but shifts of the maxima along the rotation axis indicated that the cI-mediated loops often constrained more than a proportional amount of a

molecule's overall DNA supercoiling level and modified the extension *versus* rotation response of the remainder of the DNA tether.

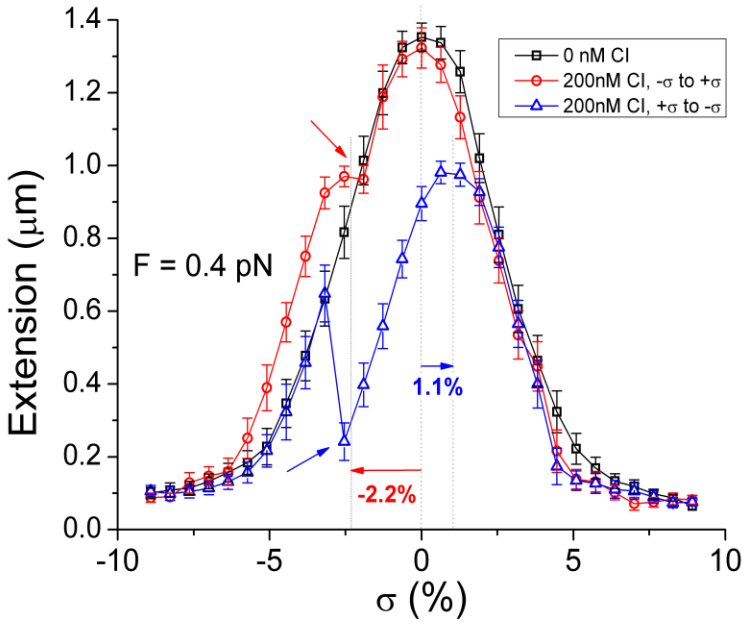

Figure 3.1. Shifted DNA hat curves with trapped supercoils. Representative extension vs. twist curves showing shifted and reduced maxima upon loop formation. Under 0.4 pN of tension in the absence of cI protein (black), a tether with a 1051 bp loop tether formed plectonemes that reduced extension for both positive and negative twist. At the same tension, in the presence of 200 nM cI protein (red and blue), as the twist in a tether was relaxed from -10% (red) or 10% (blue) superhelical density levels, reduced maxima were observed with shifts that indicated -2.2% (red) or 1.1% (blue) of the original superhelical density of the relaxed tether, Lk_0, was constrained within a cI-mediated loop. Upon rupture of the loops (arrows), the tether extension suddenly returned to unlooped values.

In the case of a tether with extensive plectonemes and operator sites separated by 1051 bp, most cI-mediated loops ruptured shortly after the twisting was reversed; the extension abruptly increased, and subsequent extension *versus* rotation data followed the unlooped

curve of the control condition (Figure 3.1, red curve). However, in a few cases, the loop did not rupture until the torque had completely reversed sign (Figure 3.1, blue *vs.* black curves) or did not rupture at all. Both negative and positive shifts were observed and the levels of superhelicity constrained in the loop varied from -10% to 16% (with respect to the looped segment, Figure 3.2). This is remarkable since plectonemes were formed by twisting only +/-10% (with respect to the entire tether); plectonemes begin to form at 2-3% supercoiling, so only 7-8% should have been localized in a plectonemic loop.

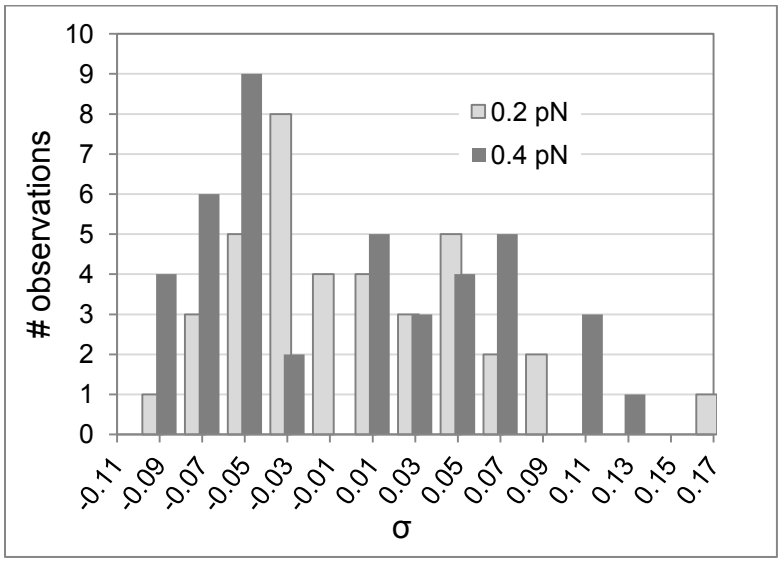

Figure 3.2. Distributions of trapped supercoils in 1051 bp loops. Levels of superhelical density constrained in 1051 bp DNA loops as shown in Figure 3.1, ranged from -10% to 16% under tensions of 0.2 - 0.4 pN. Although the tethers were only twisted to introduce between -10 and +10% supercoil density, the superhelical density indicated by the shift of curves was constrained within a DNA segment of only 1051 bp. Therefore constrained superhelical density was as high as 16%. At 0.2 pN, the constrained superhelical density levels were distributed around zero but slightly more negative values were observed. At 0.4 pN, the constrained supercoiling levels formed a broad distribution in three clusters.

In 1051 bp DNA loops, at 0.4 pN tension, the distribution of constrained superhelicity exhibited peaks at -6, 0, or +6% supercoiling level. In contrast, at 0.2 pN of tension the distribution was more continuous. Similar experiments were conducted using DNA with operator sites separated by 393 bp. Within mechanically produced plectonemes, 393 bp loops often formed which shifted the extension *versus* rotation curves upon unwinding. However, this smaller looped formed more readily and experiments at higher tension were possible. Unexpectedly, the amount of superhelicity trapped in cI-mediated loops increased with tension (Table 3.1). Tension alters the conformational equilibrium of a DNA tether under torsional strain to favor twist over writhe, and twist diffuses rapidly along DNA (54), so superhelical density should be more delocalized under tension. However, if tension reduces the number of plectonemes in the tether, the DNA supercoiling level might be restricted to one plectoneme. This would effectively localize the DNA supercoiling level, so that it can be captured more easily in a loop surrounding that plectoneme.

Tension (pN)	Trapped supercoils	N
0.2	-3.2 ± 0.8	5
0.35-0.4	-3.8 ± 3.3	5
0.44-0.51	-5.3 ± 2.3	6
0.65-0.71	-6.7 ± 3.2	3

Table 3.1. Statistics of supercoils trapped in 393 bp loops under tension. Amount of superhelicity trapped in cI-mediated 393 bp loops increased with tension. Fitting extension versus rotation curves, like those in Figure 3.1, for DNA tethers with separations between operators of 393 bp, produced estimates of the average, constrained superhelical density. N: number of observations; ±: standard deviations (S.D.).

3.2. Loops alter effective DNA elasticity

In absence of cI protein, the dependence of DNA extension on the DNA supercoiling level, σ, can be described by the analytical approach described in (41). Briefly, the method is based on the assumption that in a DNA fragment at a given tension, the degree of its supercoiling level affects its free energy.

In the presence of a cI-mediated loop, three different regimes can be defined corresponding to: (i) purely stretched DNA for $|\sigma| < |\sigma_s|$ for which $\Delta G = -g + \frac{1}{2} c_s \sigma^2$ (ii) purely plectonemic DNA for $|\sigma| > |\sigma_p|$ for which $\Delta G = \frac{1}{2} p \sigma^2$ and (iii) a mixture of the two "pure" states for $|\sigma_s| < |\sigma| < |\sigma_p|$ for which $\Delta G = \frac{-g}{1-p/c_s} + \sqrt{\frac{2pg}{1-p/c_s}} |\sigma|$ (40). In these free energy expressions, we introduced σ_0, the supercoiling level presumably trapped inside the loop after its formation, where its number fitted consistently with the superhelical density of each individual in Figure 3.2, and replaced all the σ in expressions (i) ~ (iii) with $\sigma - \sigma_0$ when the cI-mediated loop is formed and extension is shortened. For other parameters, g is the force-dependent free energy of stretched, nicked DNA and c_s is the force dependent, twist stiffness of stretched DNA. The statistical mechanical expressions for these two quantities are published (41). They both depend on the persistence lengths of DNA bending, A, and twisting, C. The constant p is instead related to the twist stiffness for plectonemic DNA, P, through the expression: $p = K_B T P \omega_0$, where $\omega_0 = \frac{2\pi}{3.6}$ nm^{-1} is used to convert the linking number to an angle of rotation per contour length. The threshold values of supercoiling that separate the three regimes can be calculated as

$|\sigma_s| = \frac{1}{c_s}\sqrt{\frac{2pg}{1-p/c_s}}$ and $|\sigma_p| = \frac{1}{p}\sqrt{\frac{2pg}{1-p/c_s}}$. In the presence of cI-mediated loop, the force derivative of the free energy gives the relative DNA extension as the linking number changes:

$$\frac{z}{L} = -\frac{\partial \Delta G}{\partial \mathcal{F}}\Delta L \qquad \text{[Eq. 6]}$$

where z is the extension measured in the extension versus rotation curve, and L is the double-helix DNA contour length. We introduced ΔL, the length shortening factor solely due to the loop formation, when fitting the relative DNA extension $\frac{z}{L}$ in looped extension versus rotation curve data.

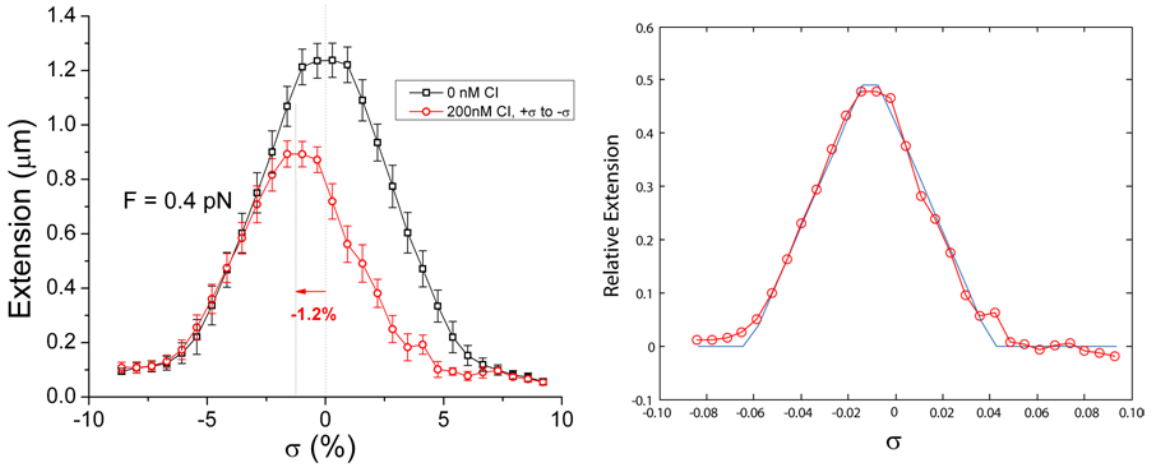

Figure 3.3. Computational modeling for shifted DNA hat curves. (Left) experimental data of extension versus rotation curve in the absence (black curve) and presence (red curve) of cI protein and its loop formation. (Right) Model fitting (blue lines) for the experimental data in the presence of cI-mediated loop (red dots and curve, same as the red curve on the left except the exclusion of the error bars).

For 1051 bp loop, using (Eq. 6) and the above parameters without replacing σ with $\sigma - \sigma_0$, across the entire range of tension investigated, the data for the extension versus rotation curves for DNA without cI protein gave satisfactory fits with A = 50 nm, C = 95 nm (Figure 3.3, Table 3.2). These values correspond well with those determined in single molecule measurements (55-57), theoretical modeling (41, 58, 59), and bulk measurements (60, 61). In the presence of cI, the extension *versus* rotation curves of tethers containing a loop were fitted using (Eq. 6) and the above parameters by optimizing the DNA length and σ_0, the shift of the extension maxima. For the looped DNA tethers, σ directly revealed the linking number constrained within the loops (Table 3.2, Figure 3.2). Similarly to measurements for nucleosome formation (62), magnetic tweezers permitted direct and quantitative measurement of the linking numbers associated with the transient cI-mediated loop in a DNA molecule.

curve	ΔL (μm)	<σ+> %	<σ-> %	A (nm)	C (nm)	P (nm)
0.4 pN looped	-0.24±0.04	5.6	-6.4	50	95	8.6±2.3
0.4 pN unlooped						11.0±1.0
0.2 pN looped	-0.27±0.04	5.3	-4.3			6.9±1.8
0.2 pN unlooped						8.3±0.9

Table 3.2. Properties of DNA elasticity change upon loop formation. Estimates of the loop size, and the average, constrained, positive or negative superhelical densities were obtained from fits of extension vs. twist curves for tethers as shown in Figure 3.2.

As shown in Table 3.2, the magnitudes of positive or negative constrained DNA supercoiling levels, <σ+> and <σ->, averaged 4-6%. The reduction in length upon loop

formation was commensurate with the size of the loop, 1051/4947 = 0.21. *P* was lower at lower tension (0.2 pN) and in the presence of looped DNA. Plectonemes are torsionally softer at lower tension (41), but also became softer when the cI-mediated loop formed (see discussion). *P* was lower than previously reported values from single molecule experiments (63), perhaps due to the higher concentration of salt in the present experiments.

3.3. Supercoiling influences the ability of lambda cI repressor to secure DNA loops

To further explore the interaction between supercoiling and loop topology, the spontaneity of looping in gently stretched tethers was characterized as a function of superhelical density for several different loop sizes.

3.3.1. Looping requires (negative) supercoiling

Loop formation and rupture was monitored in a 4397 bp DNA tether (loop length 393 bp) in the presence of wild-type cI at a concentration of 160 nM (Figure 3.4). Gentle stretching of DNA tethers obstructed looping, but as little as 0.5% unwinding enabled loop formation. When the superhelical density of DNA was positive (positive linking numbers), formation of 393 bp loops was extremely rare and short-lived. In fact, with about +1% superhelical density and 0.2 pN of tension, only 4 events, lasting about 2 s each, were observed during hours of recording. Furthermore, loops never formed in

rotationally relaxed DNA. Instead, looping occurred in negatively supercoiled DNA at tension less than or equal to 0.8 pN (Figure 3.4, upper panel).

A.

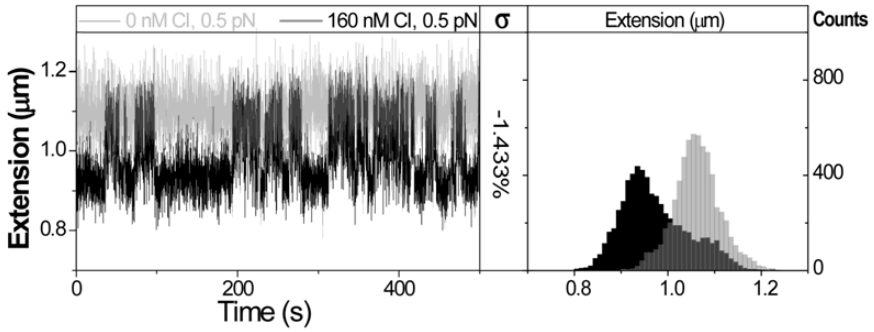

B.

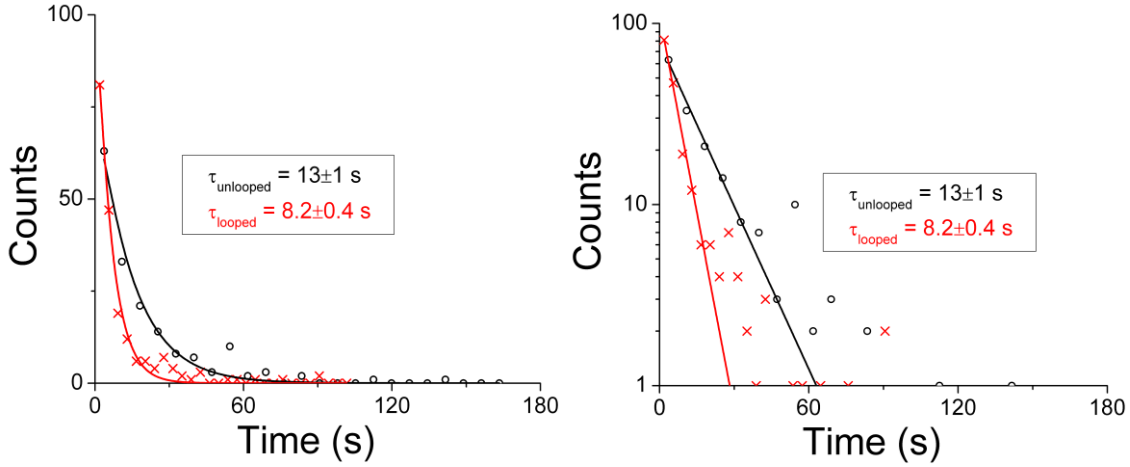

Figure 3.4. Formation and rupture of 393 bp loops mediated by cI in DNA with σ = -1.4% under 0.5 pN of tension. (A) Representative recordings of tether extension vs. time (left) exhibiting transitions in the presence of 160 nM cI (black) but not in the absence of cI (grey), and respective extension histograms (right) for single DNA tethers under 0.5 pN tension. (B) Intervals of looped (red) and unlooped (black) lifetimes for the entire set of recordings in the presence of 160 nM cI were fitted with single exponential decays to determine mean lifetimes. Original (left) and semilog (right) scale were both plotted out. Original experimental data for this particular loop size were acquired by Dr. Carlo Manzo during his postdoctoral training in the Finzi lab.

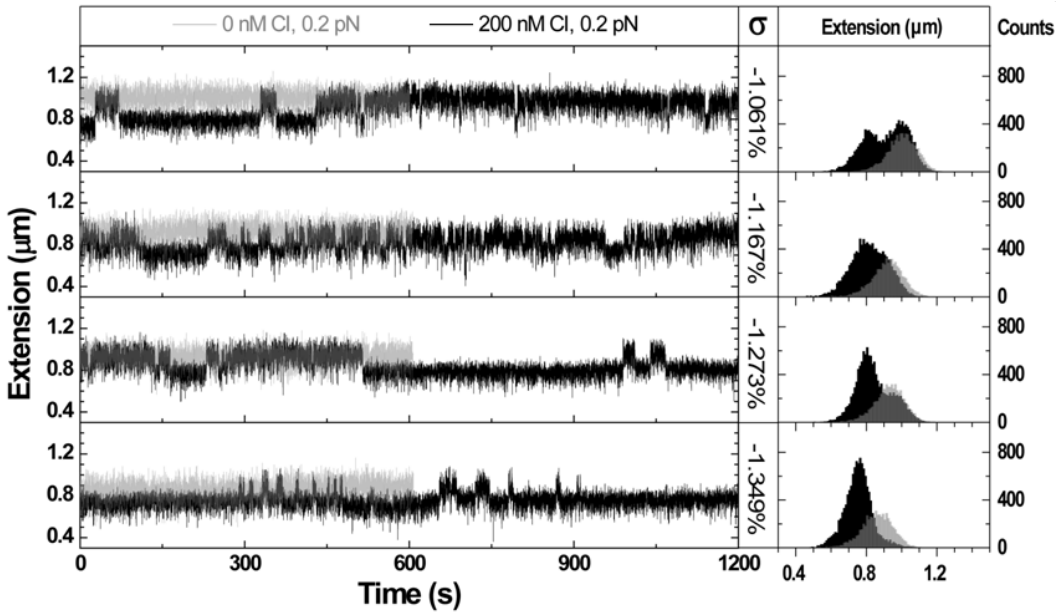

Figure 3.5. Formation and rupture of 1051 bp loops. Representative recordings of extension vs. time (left) and respective extension histograms (right) for single DNA tethers under 0.2 pN tension, showing the formation and rupture of 1051 bp loops at different supercoiling levels. In the absence of cI protein, the DNA extension was constant appearing as a single peak on the respective extension histogram. The peak corresponding to the unlooped tether shifted slightly towards shorter values as negative superhelical density increased. In the presence of 200 nM CI, the extension of the tether intermittently shifted between looped and unlooped configurations creating telegraphic signals that gave rise to two peaks in histograms. An additional -0.3% of twist was enough to shift the DNA from nearly evenly splitting time in looped and unlooped states to remaining almost always looped.

3.3.2. Negative supercoiling lowers free energy of looping

While 393 bp loops formed spontaneously even at forces of 0.8 pN, longer loops only formed at lower tension. In control traces at 0.2 pN without cI, 1051 bp loops did not

form (Figure 3.5, left panels, light grey traces). In contrast, with 200 nM cI and negative DNA supercoiling levels between -1.061 to -1.349%, spontaneous looping was observed (Figure 3.5, left panel, dark grey traces). More negative DNA supercoiling levels may also promote looping, but loops cannot be reliably distinguished when plectonemes form at such low tensions. Distinguishable, longer loops only formed under tensions less than or equal to 0.4 pN, and loop formation in even longer loops of 1231 or 1662 bp, required even lower tension. In the associated histograms, as the DNA supercoiling level became progressively more negative, the peak associated with the approximately 1 micron long, unlooped DNA tether progressively decreased while the peak corresponding to the shorter, looped form near 0.8 micron length increased (Figure 3.5, right panel).

Loop formation was significantly enhanced by further supercoiling. Extension *vs*. time recordings showing loop formation/rupture were analyzed using the "change point" algorithm (see section 2.3) to determine when the DNA extension changed significantly. Refinement with an expectation-maximization clustering algorithm allowing two states (looped and unlooped) produced a best estimate of the actual transitions between states in the recordings. The "change-point" and the expectation-maximization clustering algorithms were adapted to magnetic tweezers data from an original version developed for tethered particle microscopy (TPM) (51, 52). Based on this reconstruction, the dwell times in each of the two states were tabulated and fit as exponential distributions to determine the characteristic lifetimes of the looped (τ_L) and unlooped (τ_U) configurations (Figure 3.4, lower panel; Figure 3.6). The characteristic values of τ_L and τ_U at different forces for different values of DNA unwinding ranged between 2~35s and are plotted as

functions of DNA supercoiling level in Figure 3.7. For 393 bp looping, as σ increased, the characteristic unlooped lifetime decreased and that of the looped lifetime increased. For larger loops, the same trend was observed for unlooped lifetime, while the average looped lifetime only fluctuated around 5s.

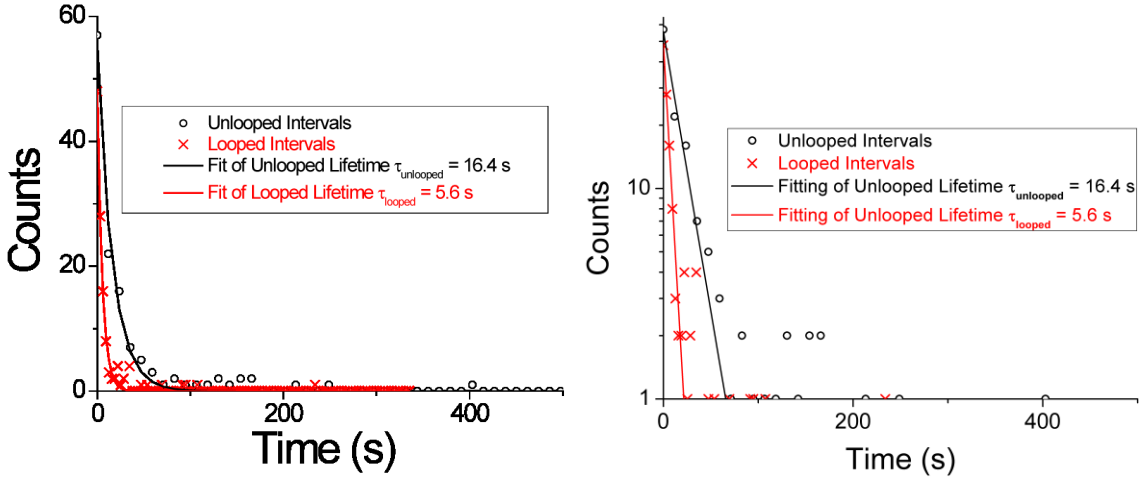

Figure 3.6. An example of calculation on DNA looping lifetimes. An example calculation of the mean lifetime for unlooped (black) and looped (red) states for a DNA tether with cI operator sites separated by 1051 bp under 0.4 pN Tension and unwound by -1.804% sigma (-8.5 turns). The lifetimes of looped and unlooped states were determined using the change-point algorithm, binned and plotted as histograms, and fitted with single exponential decay functions. Original (left) and semilog (right) scale were both plotted out.

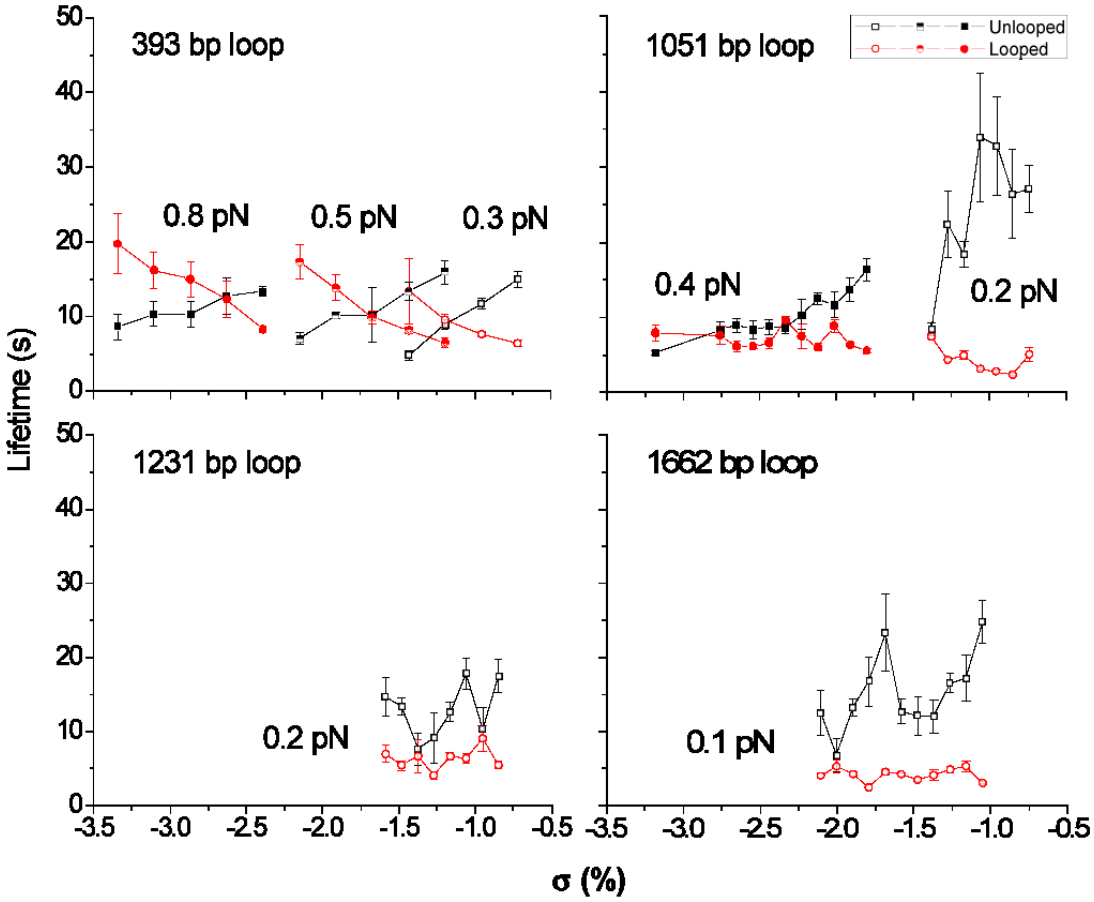

Figure 3.7. Lifetime calculation for different loop sizes. For DNA tethers under different applied tensions and supercoiling levels for different loop sizes, the calculated mean lifetimes of unlooped (black) and looped (red) states varied from 2 to 35s. For 393 bp loops, unlooped lifetime (black) decreased and looped lifetime (red) increased as the supercoiling density became more negative. For 1051 bp loops, the mean lifetime of the unlooped state still decreased as negative supercoiling increased, but the mean lifetime of the looped state fluctuated around 5s. For even larger loops of 1231 or 1662 bp, mean lifetimes fluctuated with no clear trends.

3.3.3. Negative superhelical density offsets tension to favor looping

The free energy for loop formation under specific tension and supercoiling levels was calculated using the expression $\Delta G / k_B T = - ln (\tau_L / \tau_U)$. Looping was observed only

across a narrow range of superhelical density for a given tension, because with too little negative σ, no looping occurred, and with too much, the molecule formed plectonemes making it impossible to detect looping events. However, within these limits, and especially for the 393 and 1051 bp loops at higher tension, ΔG decreased with more negative DNA supercoiling level (Figure 3.8). In fact, the level of DNA supercoiling level compensated for increased tension.

For the 393 and 1051 bp loops as the tension increased, the free energy of looping could be maintained low by unwinding the tether even further. Estimates of the free energy change for cI-mediated DNA looping *in vivo* are -3.5 kcal/mol (10, 64). This is the result of the favorable free energy change from assembly of an octamer plus a tetramer to secure the loop, -0.5 kcal/mol plus -3 kcal/mol, which compensates for the unfavorable entropy change associated with large loops. Less cooperative loop-securing proteins, like the bidentate Lac repressor tetramer, fail to achieve less than 9-10 kcal/mol free energy change *in vivo* for the sizes of loops used in these experiments (65). The *in vitro* data with loops ranging from 393 to 1632 indicates that a minimum amount of negative superhelicity lowers the ΔG by a factor of four, and further unwinding makes looping spontaneous (negative ΔG). Unwinding DNA may be the key to spontaneous looping *in vivo*.

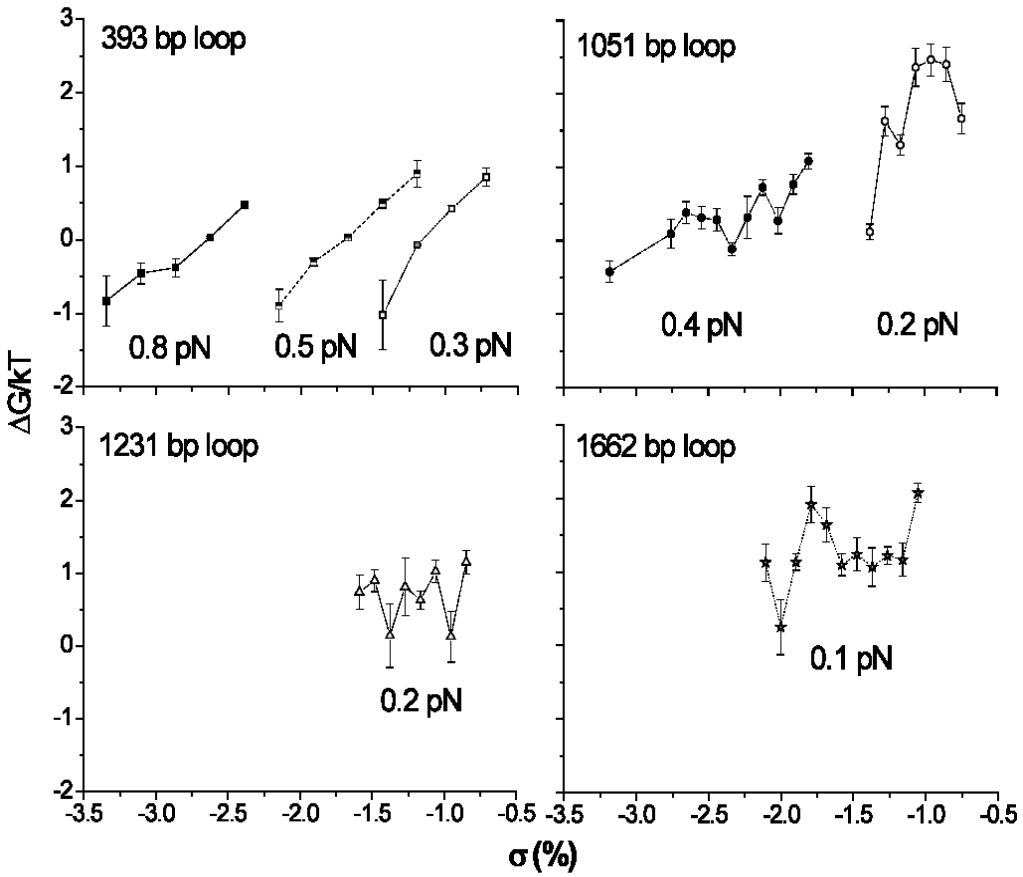

Figure 3.8. Free energy calculation for different loop sizes. The calculated free energy (ΔG) for the formation of loops under different tensions and superhelical density levels based on the lifetimes of looped and unlooped states, using $\Delta G / k_B T = - ln (\tau_{looped} / \tau_{unlooped})$. For identical loops under identical tension, more negative superhelical density decreased ΔG. This trend was clearer for smaller loops (393 bp and 1051 bp) than for bigger ones (1231 bp and 1662 bp).

3.4. Discussion

The idea that loops and genomic domains can sequester supercoiling may have important implications for regulatory processes within the loop/domain. The present data show that cI-mediated loops of wild-type length (2317 bp) can sequester superhelicity on the time scale of minutes, and that shorter cI loops are even more effective. Such cI-constituted

"insulators" could separate topologically distinct genomic domains. Furthermore quite high levels of superhelicity can be constrained in a cI-mediated DNA loop. Finally, the fact that negative superhelicity favors the formation of cI-mediated loops in DNA under slight tension suggests that the lambda phage utilizes supercoiling as a signal. Polymerases are known to be able to exert tens of pN of tension (66), much more than was investigated in the experiments presented here, and transcription can produce large values of superhelicity (67). DNA supercoiling has been shown to be a general regulatory mechanism in several organisms (68-70) and superhelical domains seem to serve as locus control mechanisms for related human genes (15, 67). These genomic observations correlate well with recent single molecule work with *E. coli* RNA polymerase, and demonstrate that number of transcriptional pausing increases and the transcription rate decreases as a function of torque in the DNA template (34). A very intriguing linkage between DNA supercoiling, nucleoid-associated proteins (NAPs), and the ordering of genes exists in bacteria and is suggested to coordinate oxygen and nutrient availability with chromosome structure (71). This body of work solidly demonstrates that excess negative linking number is a fundamental parameter in gene regulation.

In the present experiments, unwinding certainly catalyzed DNA looping into topologically distinct domains, suggesting that negative superhelicity may toggle the lytic *versus* lysogenic switch when the lambda bacteriophage infects an *E. coli* bacterium. During quiescent infection of *E. coli* by bacteriophage lambda, the lambda repressor binds to operators separated by 2317 bp causing a loop that represses transcription of cI. This DNA loop circumscribes just one promoter, but is stabilized by and can effectively

constrain negative DNA supercoiling level on the timescale of minutes. These features suggest that the phage genome has evolved to facilitate quiescent propagation through lysogeny maintained by efficient, negative supercoiling enhanced looping during favorable growth conditions for the bacteria. If oxygen and nutrients begin to diminish, so does negative supercoiling in the bacterial chromosome into which that the phage genome is inserted. Diminished DNA supercoiling level would then destabilize looping to eliminate cI auto-repression and block the switch to lysis in cells that are unlikely to be able to complete the process.

These experiments demonstrate that an archetypical regulatory loop in prokaryotic transcriptional regulation effectively divides a DNA molecule into loops of distinct superhelical densities and that loop formation is catalyzed by DNA unwinding. Such features are essential for transcriptional regulation through superhelical density, which could be the most dynamic of all epigenetic "marks". In the future, correlations of transcription and DNA supercoiling within topological domains, such as that produced by bacterial repressors, would greatly enhance our understanding of the dynamics of transcriptional regulation.

Part II: A Combined Magnetic Tweezers (MT) and Single Molecule Fluorescence Resonance Efficiency Transfer (smFRET) Instrument to Calibrate the Molecular Tension - Based Fluorescence Probes

Chapter 4 Introduction

4.1. Cellular Force: Important yet poorly understood

Mechanotransduction converts mechanical stimuli into chemical activities and plays an important role in physiological, developmental, and cellular processes (72-75). Studies during the past ten years have focused on identifying critical mechanosensitive molecules and cellular components, including stretch-activated ion channels, integrins, cadherins, growth factor receptors, myosin motors, cytoskeletal filaments, nuclei, extracellular matrix, etc (76). Despite the apparent significance of force-dependent regulation *in vivo*, understanding of this phenomenon is lagging behind. Until recently, development was made by understanding the molecular mechanisms under tension within the structural context of living cells and tissues, with direct visualization of cellular force in the mechanotransduction processes (77-79). Furthermore, little is known about the range of forces involved in mechanotransduction processes, except that most cellular force ranges within 100 pN.

4.2. Molecular Tension - Based Fluorescence Microscopy (MTFM) and its probes

Despite the efforts in understanding mechanical forces in biology, few methods are available to measure molecular forces in living systems (80-85). One of the pioneer works (80) introduced a new type of tension sensor based on fluorescence to measure mechanical tension across vinculin, a protein that connects integrins to actin filaments and has been known for its force-dependent recruitment to focal adhesions (FAs, complex intracellular linkages between integrins and the F-actin cytoskeleton). Between its N-terminal head domain and C-terminal tail region, the authors inserted an entropic

spring composed of a 40-amino-acide-long repetitive flagelliform linker motif and flanked by a pair of fluorophores, to measure the conformational changes of vinculin based on the fluorescence resonance energy transfer (FRET) readout from the N-terminal donor, mTFP1, to its C-terminal acceptor, venus. When force across vinculin extends the inserted elastic linker, FRET efficiency decreases. In this way, the authors combined tension detection with fluorescence measurement, and demonstrated the independent regulation of vinculin recruitment to FAs and force transmission across vinculin (~ 2.5 pN measured by the authors).

To measure cellular forces, the Salaita Lab developed molecular tension - based fluorescence microscopy (MTFM), a technique that allows one to visualize piconewton forces using a conventional fluorescence microscope (84, 85). In MTFM, a flexible linker (one of the polymers such as DNA or PEG) is flanked by a fluorophore and a quencher, such that tension leads to extension of the linker and significant increase in fluorescence (Figure 4.1). To calculate the applied force, the extension of the polymer is determined from the fluorescence resonance energy transfer (FRET) detection, and the worm-like chain model is then used.

MTFM provides a direct approach to map piconewton forces at the cell membrane, by measuring the ensemble force from a number of receptors per probe molecule. However, since the forces were all calculated based on worm-like chain or other theoretical model fitting to the biomacromolecules, the accuracy of obtained results was not verified and validated experimentally. Also, the force measured in cells depends on the surface

density of receptors on the cell membrane. To accurately measure the single-molecule level force applied on each receptor, concentration of the force probes needs to be tuned, and the individual probe requires accurate calibration, which is, to measure the extension of polymer used in the force probe with known applied force and obtain a force - fluorescence curve for that particular probe.

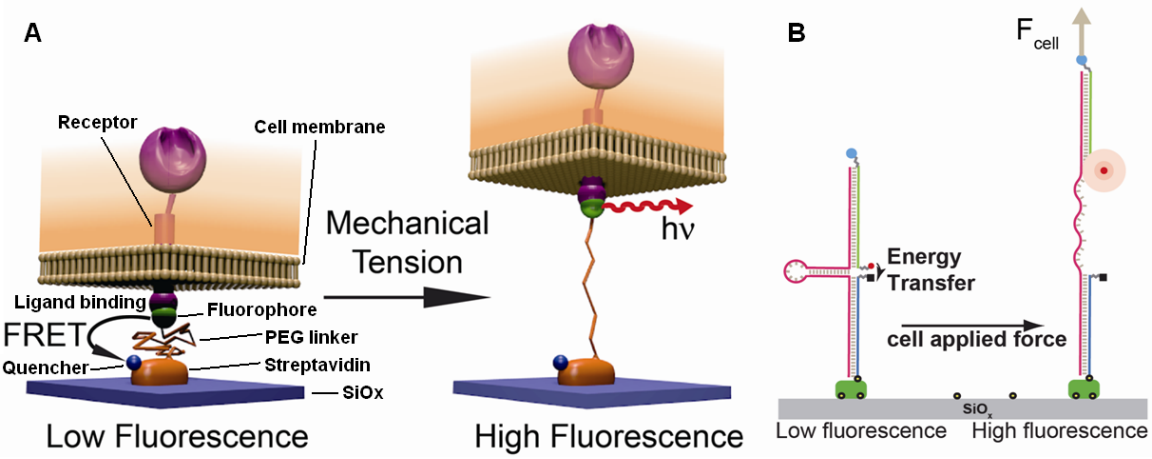

Figure 4.1. Molecular tension - based fluorescence microscopy (MTFM) probes. Schematics showing the working principle for molecular tension - based fluorescence microscopy (MTFM) probes. (A) The MTFM probe consists of a PEG linker with one end immobilized on the glass surface by a quencher-labeled streptavidin and a fluorophore-labeled ligand attached to the other end. In the absence of its respective cellular membrane receptor, the PEG linker in the probe is relaxed, and the fluorescence is quenched. Upon ligand binding on the cellular receptor, cellular force is transduced through the membrane onto the probe, rendering a gradual fluorescence increase with extension of the PEG linker. Figure adapted from (84). (B) When force is applied, the fluorescence of a DNA hairpin MTFM probe behaves in a binary state: low when the hairpin is closed (fluorophore quenched), and high when the hairpin is open (fluorophore unquenched).

4.3. Research Questions

The key problem to solve here, as mentioned above, is to accurately calibrate the MTFM probes, by quantitatively measuring the applied force on an individual probe while at the same time detecting its fluorescence change at single molecule level. This will eventually lead to a better understanding of the origin and mechanical properties of cellular forces, and their relevant roles in cellular function and regulation. Some of the main questions are, for example, what the force ranges are in mechanotransduction, and in what way molecular interactions across the membrane such as receptor clustering or aggregation affect force generation and conduction in cells. To address this issue, a single molecule technique such as atomic force microscopy (AFM), optical trap (OT) or magnetic tweezers (MT) that can generate and measure piconewton force should be integrated with fluorescence microscopy. Previous work has provided a few examples to confirm the possibilities of combining fluorescence microscope with AFM (77), OT (80), and magnetic tweezers (87-91). Due to the space limit for optical path setup, the range of force needed to generate (1-40 pN), and the instrumental difficulties for integration, AFM or OT was not considered in our case. To generate the most stable force within the required force range with relative ease of integration, magnetic tweezers become our choice of instrument.

This does not mean that magnetic tweezers do not have practical limitations. MT typically have a lower temporal resolution than OT or AFM, limited by the video-based detection, which prevents the direct measurement of very fast (ns to μs scales) or very small (Å to nm level) displacement (86). According to the spring pendulum model and

equipartition function (Eq. 3), the MT trap stiffness decreases inversely with the polymer length l, and a reduction in its stiffness leads to a reduced f_c (sampling frequency), which sets its temporal resolution. One way of compensation is to use shorter molecules at higher forces, but this is limited by the nature of our question (and thus the force range) and the requirement of avoiding autofluorescence emitted from the tethered paramagnetic beads. Since the spatial resolution is correlated with the temporal resolution, the spatial resolution of MT is also naturally restrained within a few nanometers (25).

Fortunately, the calibration of the MTFM probes with typical resolution limited by ~1 μm at 100 ms acquisition times (85) does not involve the limiting factors for fast events or small displacement detection as discussed above. The main focus of incorporating the magnetic tweezers is to exert stable, high-enough force (up to 50 pN) on MTFM probes without interfering with their fluorescence detection, with details on the difficulties and respective solutions discussed in the next chapter.

Chapter 5 Materials and Methods

5.1 Integration of Magnetic tweezers (MT) into the fluorescence microscope

To accurately calibrate the MTFM probes, we integrated magnetic tweezers to an objective total internal reflection fluorescence (TIRF) microscope for single molecule fluorescence resonance energy transfer (smFRET) - force measurement, using a pair of rare-earth magnets to apply different known forces to a DNA tether with designed length, and coupling the force information with distance information extracted from smFRET measurement. The smFRET experiments were performed following protocols similar to the previous experiments (84, 85). In sum, strands of biomacromolecule polymers such as DNA or PEG were immobilized on the surface of a microchamber at one end, internally or externally labeled with fluorescent dye pairs, and were tethered with a paramagnetic bead at the other end of the molecule. The microchamber was then placed on the stage of the fluorescence microscope. Instrumental specifics regarding the fluorescence microscope are in 5.1.2 and have been described in previous publications (84, 85). Different forces can be applied to the polymers by changing the position of magnets near the microchamber.

Several groups have designed combined magnetic tweezers with fluorescence experiments so far (54, 77, 87-91), with only a few fully integrated magnetic tweezers with fluorescence imaging system (87, 90, 91). The difficulties of the instrumentation design lie on the specifics of each individual studied system and thus vary from case to case. In general, the designed magnetic tweezers hardware should enable exerting desired range of force (here 1-50 pN) with stable alignment; illumination of the magnetic

tweezers should generate clear, stable diffraction ring pattern of the paramagnetic beads for accurate instrumental calibration of both polymer tether length and force without interfering with FRET measurement; software control for the magnetic tweezers should be modified to work compatible with the use of a commercial fluorescence microscope.

Since fluorescence comes from total internal reflection of lasers exciting from the bottom of the objective, it allows magnets to be placed either on the side of the chamber (side-pulling, utilizing chamber flow) (35) or the top of the chamber (overhead-pulling) (23) without interfering with fluorescence measurement. It was observed that many microbeads became irreversibly bound to the surface via non-specific interactions in surface flow, thus we decided to set up an overhead-pulling design to manipulate the DNA with a vertical force that lifted the DNA tethers on the paramagnetic beads, for the simplicity of hardware design and convenience of instrumental calibration, while minimizing potential non-specific interactions of the beads with the surface. The schematic of the integrated MT-smFRET instrument is shown in Figure 5.1 and the actual pictures of the instrument are shown in Figure 5.2. Based on this design, longer DNA constructs should be chosen in experiments to avoid autofluorescence from the paramagnetic bead, and thorough surface passivation for smFRET signal detection is required.

5.1.1 Set-up and illumination of the magnet tweezers

A schematic of the portable magnetic tweezers design is shown in Figure 5.1 and photos taken in its working mode are shown in Figure 5.2. We used neodymium block

permanent magnets (NdFeB) with a linear translation stage (Thorlab) to vary the relative distance of the magnets to the sample and consequently tune the magnetic force in the range of 1-50 pN perpendicular to the surface. A pair of small cubic block magnets (K&J Magnetics, B664, grade N42) were stacked and aligned on the top of another pair of big flat square-shape magnets with stronger magnetism (K&J Magnetics, BX082-N52). Both magnet pairs were separated with a piece of Teflon filling by distance of 1 mm, and were mounted on a Ø1" Optics lens holder by a homemade rotational aluminum thumbwheel with set screws that holds the cylindrical upper part of the Teflon filling. The Teflon filling was designed to be cylindrical on the top with a centered hollowed, reverse U-shape at the bottom, in order to separate the magnet pairs and allow light to go through the 1 mm space between them. The lens holder was fixed with set screws on a linear translation stage that was immobilized at the back center of the microscope eye pieces with home-made aluminum adaptor plates and controls the vertical height of the magnets head from the sample surface.

LED light source was integrated in the set-up to allow separated illumination for magnetic tweezers calibration and prevent light interference with fluorescence signal detection. A red-colored LED (Luxeon Star Rebel, 627nm, LXML-PD01-0040) was mounted on a 20mm LED base (Luxeon Star CoolBase) to provide 75 lm illumination at 700mA by connecting to a stabilized fixed-voltage DC power supply (BK Precision, Models 1680, 13.8V) and a 15 Ω Chassis mount resistor (Digi-Key, RHRC-15-ND). The LED with base was then mounted on a 20mm fiber coupling optic collimator lens with its matching hex optic holder with flat bottom (Carclo). Focused light from the collimator

then goes through the separated space between the magnets and illuminates on sample surface.

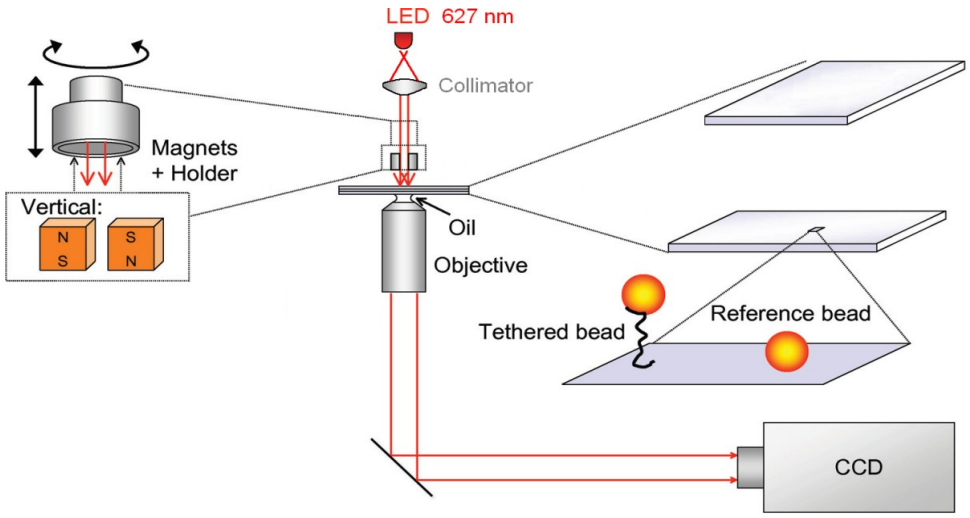

Figure 5.1. A schematic of the portable magnetic tweezers design. Figure adapted from Figure 13.1 in (24).

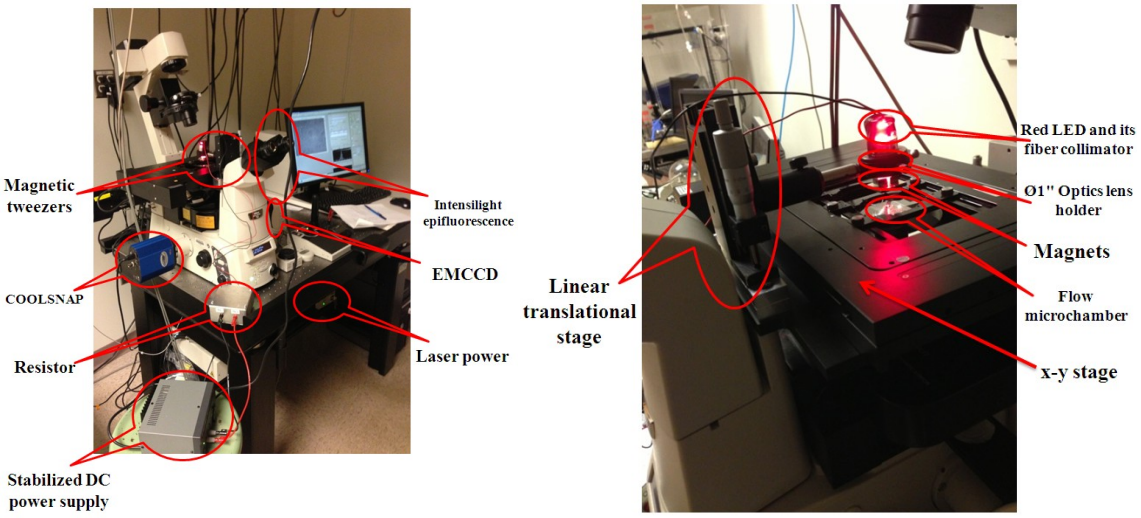

Figure 5.2. Photos of the portable magnetic tweezers instrumentation. (Left) Setup in working motion mounted on the fluorescence microscope. (Right) Zoom-in of the magnetic tweezers part over the microchamber on the stage.

5.1.2 Fluorescence microscopy system

The fluorescence microscope used in the experiment is a Nikon Eclipse Ti driven by the NIS-Elements software package. The microscope features two charge coupled device (CCD) cameras (Evolve electron multiplying charge coupled device (EMCCD), Photometrics, Tucson, AZ; CoolSNAP ES, 1392 x 1040 pixels, Photometrics, Tucson, AZ), an Intensilight epifluorescence source (Nikon), a CFI Apo 100× (numerical aperture (NA) 1.49) objective (Nikon), and a TIRF launcher with two laser lines: 488 nm (10 mW) and 638 nm (20 mW). This microscope also includes the Nikon Perfect Focus System (PFS), an interferometry-based focus lock that allowed the capture of multipoint and time-lapse images without loss of focus. The following Chroma filter cubes were also equipped in the microscope: TIRF 488, TIRF 640, FITC and reflection interference contrast microscopy (RICM).

5.1.3 Image acquisition and processing

The images are acquired from both CCD cameras with different purposes. CoolSNAP CCD has a smaller pixel number (0.06 μm/pixel) and was used in the extension and force measurements by magnetic tweezers with its LED as light source. For the calibration of DNA tether length, a 0.2μm-step z-stack series of scattered diffraction ring patterns of the paramagnetic beads were obtained at different focal planes and subsequently analyzed using homemade Matlab programs. The programs track x-y positions of the beads by 2-D Gaussian fitting to obtain the centroid position and calculate the extension of DNA-tether by comparing the intensity patterns of z-stack images from a DNA-tethered bead with

images from a stuck bead on the chamber surface in Fourier transformation. The focal plane (z grid) was then set at a fixed level and a series of scattered diffraction ring pattern bead images were obtained at different magnet positions by manually moving the magnets vertically along the y axis. Homemade Matlab programs then utilizes the calibrated DNA length from the previous step and uses the spring pendulum model (see 1.4) to calculate the force applied on the tether at each magnet position.

The EMCCD is ideal for the single molecule fluorescence measurement and was used in the measurement solely for this purpose with one of the laser beam as its light source and respective TIRF filter. Despite having a higher pixel number (0.16 μm/pixel), it has a solid state electron multiplying (EM) register that allows weak signals to be multiplied before readout noise being added by the output amplifier, thus has a high sensitivity for photon counting and not limited by the readout noise of the output amplifier even when operated at high readout speeds.

Images taken from both cameras were saved in .nd2 format and then transformed to .tiff format using the software of either ImageJ or the Nikon NIS-Element ND2 bio-formats reader. Fluorescence images taken by the EMCCD were then analyzed by ImageJ to extract background fluorescence, calculate point fluorescence maximum intensity, or statistically analyze the distribution of single molecule fluorescence.

5.2 Design of lambda DNA constructs for cellular force probe calibration combining MT-smFRET experiments

As mentioned in the previous section, to minimize autofluorescence from paramagnetic beads in general, DNA constructs were formed in a similar fashion as Chapter 2.1 described by tether segments of ~13.4 kbp lambda DNA (central DNA fragments) ligated to dye-labeled (Cy5, fluorescein or Alexa647) MTFM sensor and digoxigenin-labeled attachment fragments at opposite ends using T4 DNA ligase (New England Biolabs, NEB). Schematic of the construct with the DNA hairpin sensor is shown in Figure 5.3. The 4.4 micron lambda-DNA central fragment is linked on one end with a Cy5-QSY21-labeled 28mer DNA hairpin tension probe and immobilized on a PEG surface, and the other end is ligated with a 1 μm long multi-digoxigenin labeled DNA tail and attached on a 2.8 micron anti-digoxigenin coated paramagnetic bead (Figure 5.3). The dye-labeled DNA hairpin fragment was made by a 28-base hairpin single strand DNA with an extra triple-T single base addition at the end of its hairpin region for rigidity support (5'-GTGAAATACCGCACAGATGCGTTTGCGCGCGCGCGCTTTTGCGCGCGCGCGC TTTAAGAGCGCCACGTAGCCCAGC-3') and then annealing with its two 24mer complementary single strand DNA, one upper strand coupling with QSY21 and one lower strand coupling with Cy5, creating a NgOMIV-cut sticky end to ligate with the central DNA fragment. The digoxigenin-labeled end fragment of ~1000 bp was created using the same protocol provided in 2.1 with the primer pairs and templates listed in Table 2.3 and Table 5.1. Enzyme digestion by XhoI was then used to generate complementary ends for ligation to the central DNA fragment, which was digested by XhoI and NgOMIV from full length λ DNA. After ligation for the full construct under

16˚C overnight, the construct was filtered twice with Amicon Ultra-0.5 mL Centrifugal Filters (100kDa for DNA and Proteins, Millipore) before use.

Amplicon / Product	**Labeled Nucleotide**	**Plasmid template**	**Forward Primer**	**Reverse Primer**	**Restriction Site**
XhoI-digtail	dig-dUTP	pBluKSP	S/pUC19/2412	A/pUC19/1435	XhoI
4.4 μm Central DNA Fragment	--	full λ DNA (48.5 kbp)	--	--	XhoI & NgOMIV

Table 5.1. Reagents for central and attachment fragments in MT-smFRET experiments.

The DNA constructs were attached at one end to the streptavidin-biotin glass surface of a flow chamber and at the other end to a 2.8 μm-diameter anti-digoxigenin-coated, paramagnetic bead (use anti-digoxigenin from mouse, Roche #11333062910, coated on Dynabead Protein G from Invitrogen/Life Technologies, details described in 5.4).

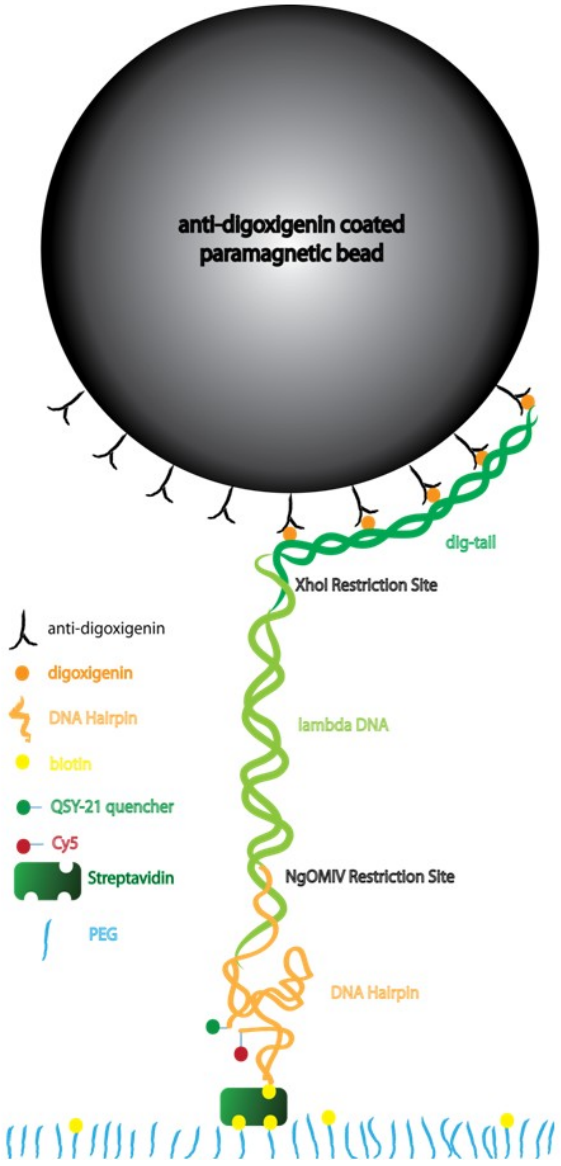

Figure 5.3. A schematic of the MT-smFRET DNA construct design, with the DNA hairpin probe.

5.3 Functionalization of coverslip chambers (surface passivation)

The protocol for functionalizing one side of the coverslip surface was adapted from previous publications (84, 85) and adjusted for optimal experimental results.

Glass coverslips were cleaned in a 5-column glass slide rack with Milli-Q® (MQ) water for 10 minutes and sonicated in acetone for another 10 minutes. They were then dried in the oven for a few minutes before etching with Piranha solution (H_2SO_4: H_2O_2 (v/v) = 35: 15) for 15 minutes to create excessive hydroxyl group (-OH) on the surface. The acid-treated coverslips were then rinsed with MQ water for at least five times to stop the reaction and subsequently sonicated in acetone for a few seconds. After rinsing the coverslips with acetone for another three times, add amine group ($-NH_2$) and passivate the surfaces with PEG monolayer by treating for 1 hour in acetone solution containing 1% silane APTES (Gelest, SIA0610.0-25GM) and 7-12 unit short PEG (Gelest, SIM6492.72-25GM). The APTES-treated coverslips were then sonicated for a few seconds and rinsed for 2-3 times with fresh acetone, followed by blow drying in N_2 stream and heating in the oven for another 10 minutes to create an evenly connected PEG monolayer surface. If not used immediately, cooled coverslips can maintain their function for another 1-2 days in a dry, sealed environment. The last step is to couple NHS-biotin on the surface via reacting with $-NH_2$ groups. This can be achieved by soaking one side of the coverslips in 2 mg/mL NHS-biotin solution diluted with dry DMSO and incubating for at least 4 hours under room temperature or overnight in a cold room before use. The coverslips can then be rinsed with acetone and dried in nitrogen stream. They can be stored under room temperature in a dry, sealed environment for a maximum of 2-3 days without jeopardizing its optimal function.

5.4 Functionalization of paramagnetic beads

In the force-fluorescence measurements, some of the DNA construct designs require biotin end-labeling on the chamber surface. To obtain heterogeneity of chemical modification at the two ends of the DNA for experimental convenience, additional chemical modification of the paramagnetic microspheres with anti-digoxigenin were introduced for specific binding to the digoxigenin-modified end of the DNA construct, besides the common use of streptavidin-coated paramagnetic beads for specific binding to the biotin-modified end of the DNA construct.

5.4.1 Preparing Beads

Dynabeads® Protein G (Life Technologies, 10003D) were resuspended from stock by vortexing for 30 seconds or tilting and rotating for 5 min. Then 50 μL (1.5 mg) of the Dynabeads® were transferred to a tube, and the beads were separated from their original solution by placing the tube on a permanent magnet and carefully removing the supernatant, leaving concentrated beads only inside the tube.

5.4.2 Binding Anti-digoxigenin

Anti-digoxigenin was diluted in 1X PBS buffer (pH 7.4) with 0.02% Tween-20 to a final concentration of 40 μg/ml before mixing with the concentrated paramagnetic beads prepared from previous steps. The mixture was incubated with rotation for 10 min at room temperature, and then the beads were washed by placing the mixture on the magnet and removing the supernatant. The beads-anti-dig complex was then rinsed twice with 200 μl 1X PBS solution containing 0.02% Tween-20. The anti-dig-conjugated Dynabeads

were subsequently stored in 1X PBS with 0.1% Tween®-20 at 4˚C to prevent aggregation.

5.4.3. DMP Crosslinking

To avoid co-elution of anti-dig with digoxigenin when binding to the dig-tail, it is necessary to crosslink anti-dig to the Dynabeads® before use in a magnetic field. Available crosslinking reagents include Bis[sulfosuccinimidyl] suberate (BS_3) (protocol from Dynabead®) and dimethyl pimelimidate•2 HCl (DMP) (87; protocol adapted from Pierce Biotechnology). Here DMP crosslinking is adopted for practical convenience.

Fresh crosslinking buffer solution was prepared as 5ml 0.2M triethanolamine (TEA), pH adjusted to 8.0. DMP was then diluted to a final concentration of 5 mM in 1 ml crosslinking buffer. Anti-dig-coupled beads were washed twice in 200 µl crosslinking buffer on the magnet. Supernatant was removed and beads were resuspended in 200 µl of 5mM DMP. They were then incubated at room temperature for 30 min with tilting / rotation. Quenching of the crosslinking reaction was accomplished in a solution of 50mM Tris-HCl (pH 8), before the beads were incubated at room temperature for 15 min with tilting/rotation. The cross-linked beads were then ready to use after rinsing for 3 times with 200 µl PBS with 0.1% Tween-20 on the magnet and discarding the supernatant.

5.5 DNA manipulation: Calibration and force - extension measurement in MT-smFRET experiments

With the surfaces dried clean and ready to use, chambers were prepared by sealing two pieces of treated glass coverslips together with their treated surfaces face-to-face in a cross shape, using grease and double-sided scotch tape to create the boundary of a channel (Figure 5.2). The channel of each chamber was rinsed with 200 µl PBS with 0.02% Tween-20, and then with 200 µl PBS buffer for twice. 1µl of prepared anti-dig beads were then mixed with 40 µl PBS buffer and injected into the chamber before incubating for 10 minutes. Each chamber was then rinsed with 200 µl PBS buffer, and followed by another 3-6 hours of incubation at 4˚C in ~50 µl of 100 µg/ml streptavidin solution in a sealed, moist environment to prevent the chamber from drying. The chambers were then examined under the microscope with the EMCCD camera to ensure that each surface existed minimal spots (< 10 spots per field of view) of non-specific fluorescence.

Before taking the chambers out of the cold room, 2-4 µl of the prepared DNA were mixed with 40 µl PBS buffer in a tube for each chamber. The mixture was then injected into the chamber and incubated for 1 hour after rinsing each with 200 µl PBS buffer for 3 times. During the incubation, 200 ml of imaging buffer was prepared per chamber containing 1X Tris buffer (20 mM Tris, pH 8.0, 50 mM NaCl), 2 mM Trolox, and an oxygen scavenging system consisting of 2.5 mM PCA (protocatechuic acid) and 50 nM PCD (protocatechuate-3,4-dioxygenase) (92). Comparison of the oxygen scavenging effect between the PCA/PCD system and the previously commonly used GODCAT (~56 mM

glucose, 100 nM glucose oxidase, 1.5 μM catalase) system were performed with different imaging buffers (Tris buffer and lambda buffer), resulting with better and more stable performances from the former (data not shown).

After incubation, freshly prepared imaging buffer was injected into the chambers before setting up the instrument with COOLSNAP CCD on and magnetic tweezers held tight on the microscope. The magnetic tweezers were aligned, its LED light was turned on, and the magnets were set to the position of ~13mm on the translational stage. Possible tethers were found by observing different diffraction ring patterns between the stuck bead ("reference bead") and the tethered DNA bead. A rough calculation on the length of the tether can be accomplished by changing z grid between the focal plane of the tether bead and that of the stuck bead, until the diffraction ring pattern for the tethered bead at one z plane is almost identical to that of the struck bead from another z plane. The length of the tether equals to the vertical displacement between these two planes. Tethered beads with lengths around 3-4 μm were considered as tethers of interest. For calibration, the magnet position was set to ~15 mm on the translational stage, and protocol described in 5.1.3 was followed. Z-stack measurements were taken in a distance change of 6 μm, starting from a position slightly above the central plane of the tether bead. After measurement, a 10-minute video with 1 frame / minute interval was taken for thermal drift detection; usually the microscope is thermally stable after 8 hours and the drift should be minimal. For force measurement, videos containing at least 20 images were taken at individual magnet positions ranging from 11 mm to 20 mm on the translational stage, and measurements were repeated at various magnet positions with minimal interval of 0.5 mm. The images

were then processed with offline ImageJ and Matlab software to calculate DNA extensions and forces at different magnet positions. Finally, the force - extension curve was plotted in Matlab and fitted with worm-like chain model using nonlinear least squares fitting method and trust-region optimization algorithm, with the persistence length P set around 50 nm. Fitting results were evaluated by the goodness-of-fit statistics mainly by examining the value of adjusted-R^2. The force - extension data should be comparable to that of the worm-like chain model, with expected value of adjusted-R^2 no less than 0.95.

5.6 Coupling single molecule fluorescence measurement in MT-smFRET experiments

Once the tether of interest was found and both force and tether extension data were recorded at different magnet positions with a satisfactory force - extension curve fitting, the magnet position was adjusted to apply force of ~1 pN on the tether and then the LED light on the MT was turned off. EMCCD was switched on and the focal plane was set on the chamber surface by achieving a crisp, edge-distinctive view of the RICM field. Then the 638 nm laser was turned on, so was the TIRF 640 filter cube; all the ND filters were off. The position of the tether was recorded before moving the stage horizontally to a neighboring field. The angle of the light was adjusted to be slightly bigger than the TIRF angle, so that both the autofluorescence spots of the stuck beads and the single-molecule fluorescence spots on the surface were easily observed. The perfect focus system (PFS) was turned on and the focal plane was manually adjusted until images with clean and clear single molecule fluorescence spots were observed (Figure 6.1). The microscope

setting conditions were saved and the PFS system was locked before switching back to the same field with the tether. Before starting the experiment, an RICM image of the field with both the tether and stuck beads nearby was captured to ensure that the focus was on the surface.

A short video containing 10 images was taken (under 300 ms or 500 ms exposure time), and then compared with the previous RICM image to identify isolated fluorescence spots within ~2-3 μm radius of the tether center. Fluorescence intensities for those spots were then measured to identify those spots with approximately single-molecule level of fluorescence (spots of interest). Magnets were subsequently lowered on the surface so that a bigger force (for example, ~17 pN in the case of the DNA hairpin MT construct) was applied on the tether. After retaking the video at the same field of view with the bigger force, fluorescence intensity on the spots of interest were re-measured and compared to their respective values in the previous video, to examine if the fluorescence on any of the spots has been significantly increased. If comparing frames were taken under different exposure times, fluorescence intensities were normalized at 500 ms exposure time using dark pixel intensity (93). When increase of the fluorescence intensity was observed for a single spot, measurements on this particular spot were repeated at different levels of force between the previous two values (in our case here, between 1~17 pN). After the experiment, background fluorescence was subtracted and changes in the fluorescence intensity of the identified spots were analyzed using ImageJ as described in 5.1.3, by measuring the maximum fluorescence value in the isolated area around each spot for each frame and plotting out the curve of fluorescence intensity *versus* time. For

the DNA hairpin MT construct, a clearly binary fluorescence change was observed around the region of its rupture force, while for the PEG probe, gradual fluorescence increase should be observed with force increase.

Chapter 6 Results and Discussion

6.1. Determining fluorophore concentration: Statistics for a single molecule experiment

To determine the fluorophore concentration for single molecule measurement, and to measure the fluorescence level of a single Cy5 fluorophore under optimal settings of microscope and filter, fluorescence experiments without force (no magnetic tweezers set up) were performed with unquenched Cy5 DNA hairpin in a 8-room plastic chamber on a biotin-PEG surface prepared with method used in (80). The molar ratio of biotin / PEG used to coat the surface is 0.074, and the hairpin concentration varied between 1 - 100 pM in different rooms of the chamber. We found that a maximum of 5 pM concentration allowed the separation of single distinct spots. These are likely single molecules, as confirmed by a single Gaussian-fit peak for >1000 spots in the field (Figure 6.1), using 1s exposure time and ND8 filter on, with the fluorescence level of a single fluorophore at ~14000-15000 i.u. in the center of the peak (Figure 6.1). This value is changed due to minor adjustment of the microscope setting, filter setting, exposure time, and TIRF angle, but rough measurement for individual spots were performed before each MT - smFRET experiment to ensure that the fluorescence detected was from single molecules. Time-lapse measurements for 1 minutes were also performed and the single-step photobleaching of unquenched Cy5 was observed for multiple molecules (Figure 6.1), confirming the existence of Cy5 at single molecule level.

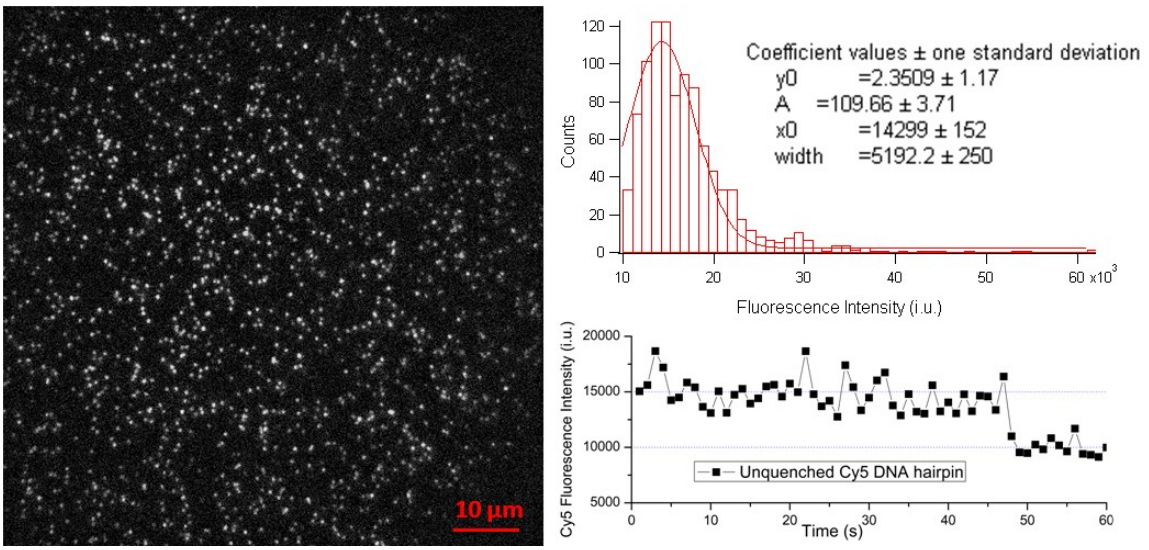

Figure 6.1. Single molecule fluorescence test. Single molecule dye intensity measurement for surface-immobilized unquenched Cy5 DNA hairpin. [biotin] / [PEG] = 0.074; [DNA] = 5 pM.

6.2. Calibrating a DNA tether: Force - extension curve on the TIRF microscope

Before the force - extension measurement for the DNA tether, we first confirmed that the DNA tether is sufficiently long to avoid autofluorescence from the paramagnetic beads even under small force (Figure 6.2). Apparently, the TIRF channel 640 (labeled as TIRF, 647 nm) is better than TIRF channel 488 (labeled as TIRF, 488 nm) in respect to avoiding autofluorescence intensity from the bead. For TIRF 640, the autofluorescence from the DNA tether is minimal even under a small force of 3 pN.

Following the protocol described in 5.5, we measured force - extension curves for > 10 molecules between 0.2 ~ 20 pN. As shown in the inset of Figure 6.3, images for the diffraction ring patterns are crisp and clear. The force - extension data (Figure 6.3, blue square) shown here is indeed comparable to that of the worm-like chain model (Figure 6.3, red curve), yielding a robust fitting by trust-region algorithm with adjusted R^2 =

0.98 > 0.95. The DNA extension is longer than expected due to the repeated pulling on the tether, resulting in partial dissociation of the anti-digoxigenin - digoxigenin tail from the paramagnetic bead surface. The force - rotation curve allows us accurately measure force within 10% accuracy with a set extension of the polymer.

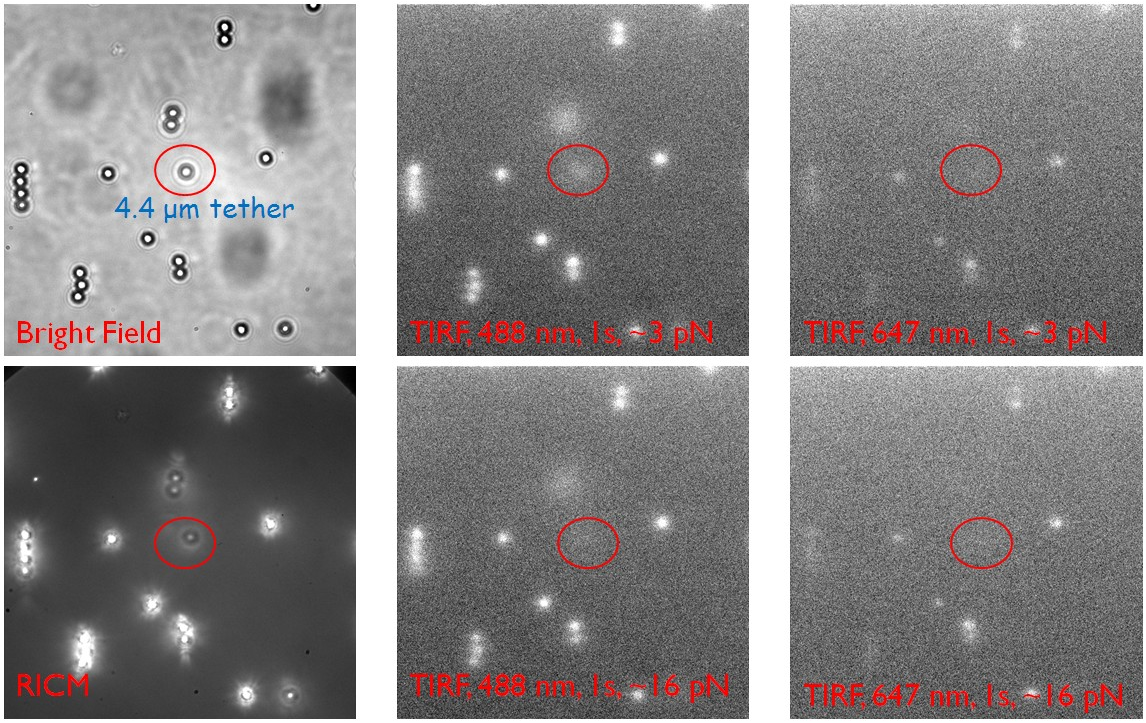

Figure 6.2. Autofluorescence control experiment for the tether. Autofluorescence is minimal in TIRF 640 (labeled as TIRF, 647 nm) under force ~3 pN.

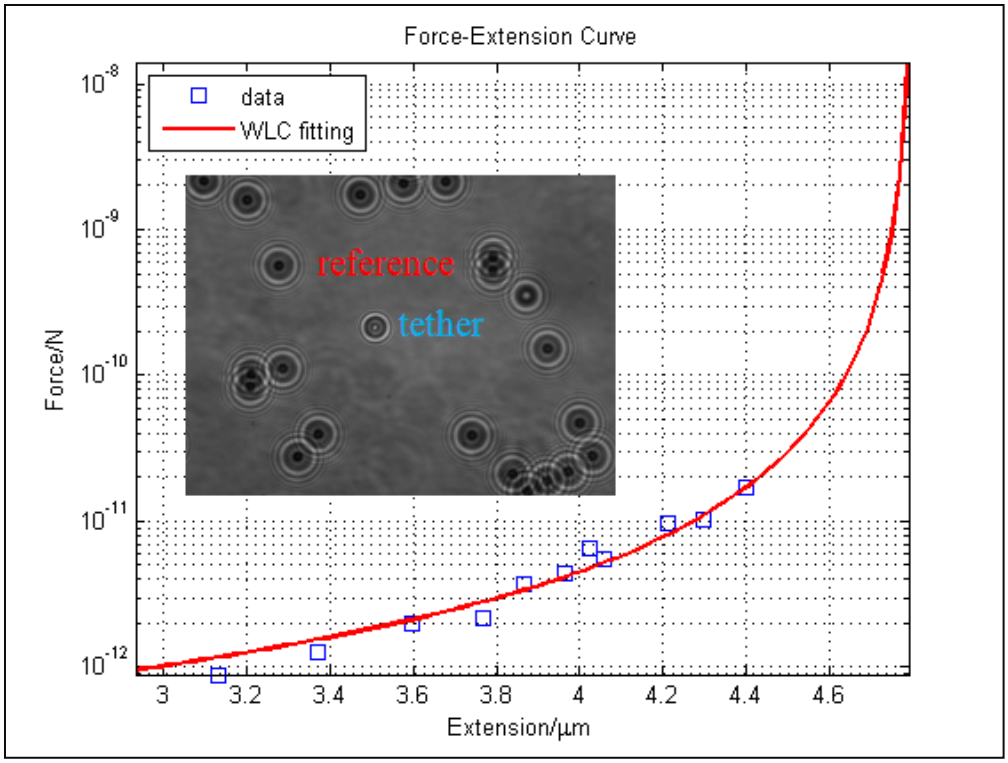

Figure 6.3. Force *vs.* extension curve of the MT-smFRET DNA construct. Force - extension curve for the 4.4 μm DNA with the linkage of DNA hairpin sensor after multiple pulling. The forces range from 0.2 pN to 20 pN and the curve fits relatively well with WLC model, with adjusted-R^2 = 0.980. Extrapolation of the WLC fitting gives estimated contour length for the DNA, which is slightly longer than expected, likely due to the dissociation of the bead and the dig-tail DNA.

6.3. Proof of concept: Binary fluorescence change with the open and close of a DNA hairpin

The opening of a DNA hairpin is induced by force at piconewton range, and for the particular DNA hairpin we used here (sequence in 5.2), its sequence-dependent force magnitude $F_{1/2}$ was calculated to be around 16 pN theoretically (94), and was measured to be 13.7 pN using micropipetting technique (Zhang et al., under revision). Using magnetic

tweezers to apply forces ranging from 1-20 pN, we observed the significant fluorescence intensity increase of Cy5 coupled with force increase (Figure 6.4, upper panel, comparing the image captured under 1 pN and 17 pN). Based on the data, fluorescence intensity could increase from ~10,000 i.u. to ~22,000 i.u. at the force of 17 pN, rendering the possible range of expected $F_{1/2}$ in between 13 pN and 17 pN (Figure 6.4, lower panel). This is consistent with the theoretical calculation and previous experimental result using the same DNA hairpin but an alternative technique with no fluorescence measurement suggesting that the signal change is likely due to its being pulled away from the QSY21 quencher. This binary intensity change can also be repeatedly observed when cycling changing the force between 1 pN and 17 pN on a DNA hairpin (Figure 6.5), as another piece of supportive evidence, although more data on different hairpin molecules under varied forces are needed to confirm the reproducibility of this result.

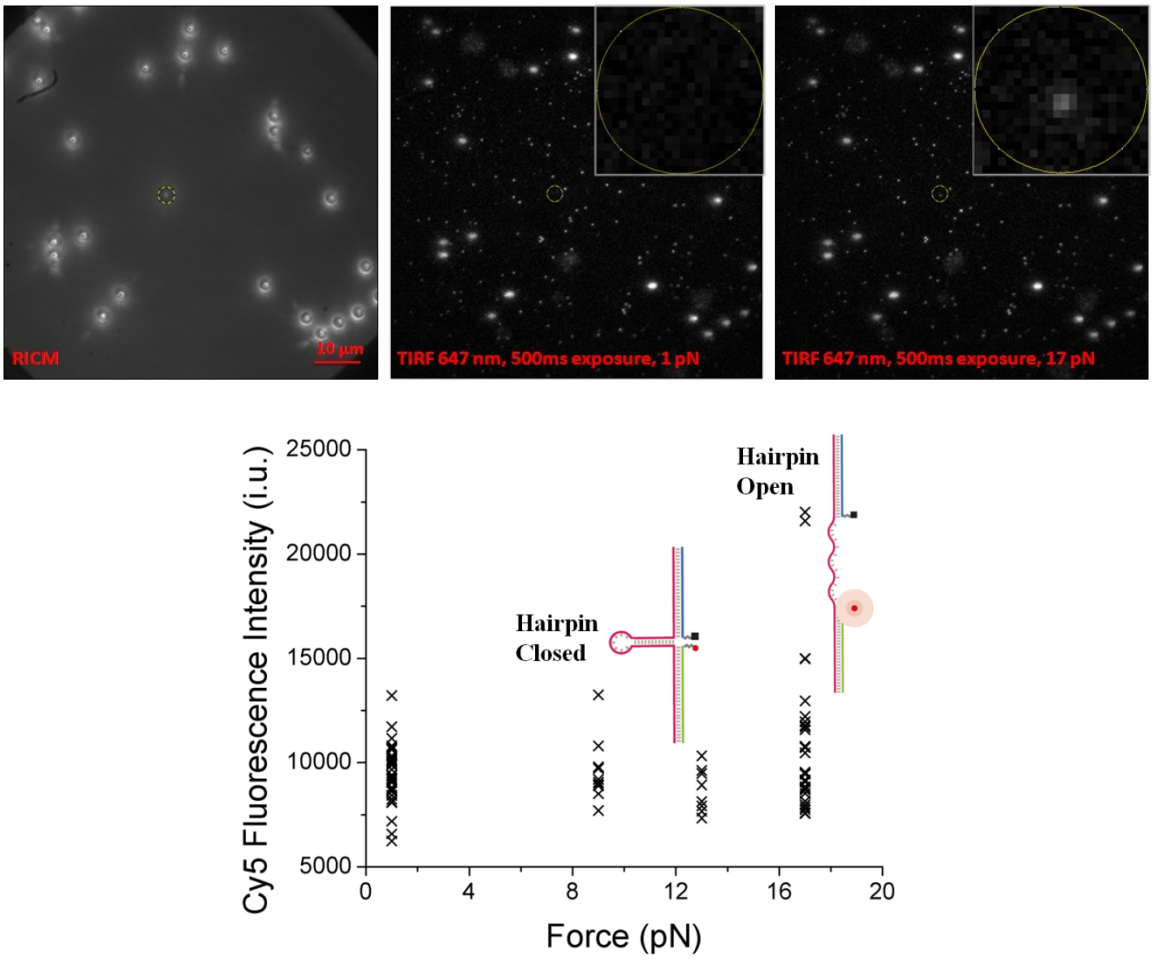

Figure 6.4. Fluorescence *vs.* force for a DNA hairpin probe. Significant fluorescence intensity increase to ~22,000 i.u. observed at high force (17 pN) comparing to the relatively low background fluorescence ~ 10,000 i.u. at low forces (1 pN, 9 pN, 13 pN) in smFRET-MT experiment. This showed a binary fluorescence change which is likely due to the repeatable opening and closing of the Cy5 DNA hairpin under different forces, with expected $F_{1/2}$ between 13-17 pN. Top: Fluorescence is low under low force, and high under high force. Bottom: fluorescence intensity change with time. Notice that under the force of 17 pN, other than the bright fluorescence signals observed at ~22,000 i.u., fluorescence signals with intensities around ~10,000 i.u. were also observed, which is likely due to the dynamic opening and closing of the hairpin, and/or the instability of the Cy5 dye.

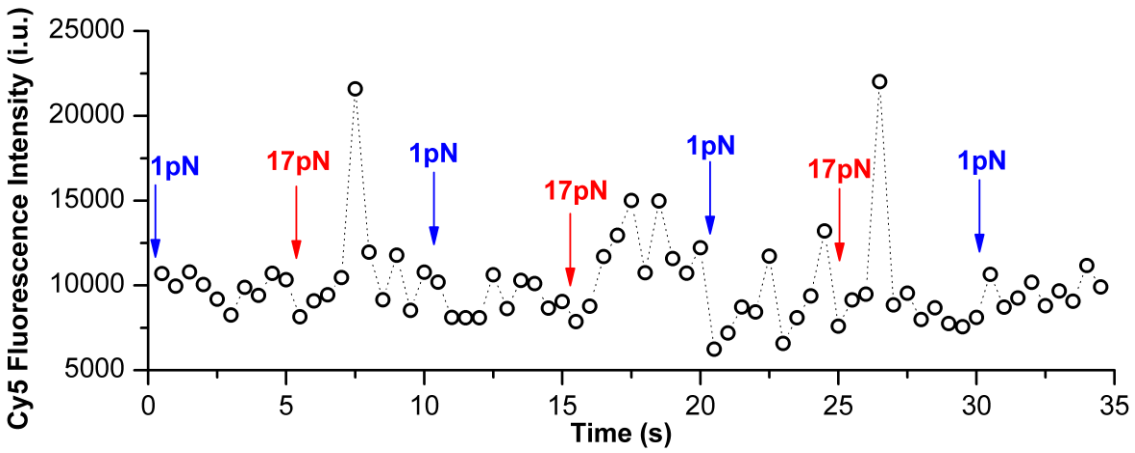

Figure 6.5. Fluorescence change with time under tension for a DNA hairpin probe. Distinct force-induced fluorescence change between 22,000 i.u. and 10,000 i.u. was repeatedly observed in a Cy5-QSY21 DNA hairpin, by changing the force between 1 pN and 17 pN in a cycling fashion. This suggested the reversible opening and closing of a Cy5 DNA hairpin during the force cycles.

6.4. Future work

More data generated by repeating the DNA hairpin experiment can confirm the stability of this technique and provide more precise details on the $F_{1/2}$. Ultimately, this method can be used to calibrate other MTFM tension probes such as the PEG-based tension sensors and gold nanoparticle tension sensor with continuous fluorescence change. Magnetization geometry could be improved for pursuing even higher force, but force applied by the current setup should be large enough (up to at least 50 pN) to measure cellular forces via ligand-receptor interactions. To improve the yield of total number of tethers on a surface and lower the experimental error due to non-specific attachment and dissociation, further advances could be made by adopting optimized methods for surface functionalization and optimal conditions for washing buffer to withstand higher force and prevent surface

contamination. One method for optimal immobilization and attachment process was developed by Janissen et al. (95) using coating beads with heterobifunctional poly(ethylene glycol)-linker (NHS-PEG-$COOH_{MW3400}$), (NHS-PEG-$Aldehyde_{MW800}$), or (NHS-PEG-$Maleimide_{MW3400}$). Covalent immobilization of different molecules was achieved via a one-step direct coupling with EDC (1-ethyl-3-(3-dimethyl-aminopropyl) carbodiimide) or a two-step indirect coupling with pre-activated carboxylic groups through EDC/NHS-activation. The method also demonstrated better surface amination in respect to the overall binding rate and homogenous coating through silanol group esterification with ethanolamine hydrochloride instead of the traditional amino silane (APTES). This optimized protocol renders stable attachment for > 8 hrs of polymer tethers under forces at 140 pN (personal communication with R. Janissen). Further experiments will benefit from adaptation of this protocol to the MTFM system.

Chapter 7 Conclusions

In part I, we showed that DNA supercoiling is a regulatory signal for the genetic switch in bacteriophage lambda that can influence the ability of lambda cI repressor to secure its mediated loop, by lowering the free energy of looping. Increased negative supercoiling compensate with the increased tension to favor loop formation. When the loop is formed, it alters effective DNA elasticity, especially shortening its twisting stiffness. In addition, this loop can constrain high levels of supercoiling, varying from -10% ~ 16%, much higher than the supercoiling level we manually introduced to the whole DNA fragments. This provides an explanation at the molecular level on how bacteriophage lambda made its switch from lysogenic to lytic stage under low energy when less negative supercoiling level could be maintained *in vivo*.

In part II, we suggested a simple instrument with protocols combining smFRET measurement and magnetic tweezers force - extension measurement to accurately calibrate the fluorescence-based DNA hairpin tension probe, by directly observing the force-induced fluorescence intensity change which is likely due to the opening and closing of the hairpin; it will eventually result in a relationship between force and FRET efficiency, given more data collected to confirm the reproductivity of this method. In the future, we would like to apply this method to other MTFM tension probes such as the PEG-based tension sensor and gold nanoparticle tension sensor. This simple and direct measurement of force-induced extension change provides a good tool for determining cellular force with higher accuracy.

References

[1] Hunt NG and Hearst JE (1991) Elastic model of DNA supercoiling. J. Chem. Phys. 95 (12), 9329-9336.

[2] Lia G, Bensimon D, Croquette V, Allemand JF, Dunlap D, Lewis DE, Adhya S, and Finzi L (2003) Supercoiling and denaturation in Gal repressor/heat unstable nucleoid protein (HU)-mediated DNA looping. Proc Natl Acad Sci USA. 100(20):11373-11377.

[3] Lia G, Semsey S, Lewis DE, Adhya S, Bensimon D, Dunlap D, and Finzi L (2008) The antiparallel loops in gal DNA. Nucleic Acids Res. 36(12):4204-10.

[4] Travers A and Muskhelishvili G (2005) DNA supercoiling - a global transcriptional regulator for enterobacterial growth? Nat Rev Microbiol 3(2): 157-69.

[5] Lilley DM and Higgins CF (1991) Local DNA topology and gene expression: the case of the leu-500 promoter. Mol Microbiol 5(4): 779–783.

[6] Chen CC and Wu HY (2003) Transcription-driven DNA supercoiling and gene expression control. Front Biosci 8: d430-9.

[7] Drolet M (2006) Growth inhibition mediated by excess negative supercoiling: the interplay between transcription elongation, R-loop formation and DNA topology. Mol Microbiol 59(3): 723-30.

[8] Brooks TA and Hurley LH (2009) The role of supercoiling in transcriptional control of MYC and its importance in molecular therapeutics. Nat Rev Cancer 9(12): 849-61.

[9] Case ED, Peterson EM, and Tan M (2010) Promoters for Chlamydia Type III Secretion Genes Show a Differential Response to DNA Supercoiling That Correlates with Temporal Expression Pattern. J Bacteriol 192(10): 2569–2574.

[10] Dodd IB, Shearwin KE, Perkins AJ, Burr T, Hochschild A, and Egan JB (2004) Cooperativity in long-range gene regulation by the lambda CI repressor. Genes Dev 18(3):344-354.

[11] Zurla C, Manzo C, Dunlap D, Lewis DE, Adhya S, and Finzi L (2009) Direct demonstration and quantification of long-range DNA looping by the lambda bacteriophage repressor. Nucleic Acids Res 37(9):2789-2795.

[12] Manzo C, Zurla C, Dunlap DD, and Finzi L (2012) The effect of nonspecific binding of lambda repressor on DNA looping dynamics. Biophys J 103(8):1753-1761.

[13] Filipski J, Leblanc J, Youdale T, Sikorska M, and Walker PR (1990) Periodicity of DNA folding in higher order chromatin structures. EMBO J 9(4):1319-1327.

[14] Gibcus JH and Dekker J (2013) The Hierarchy of the 3D Genome. Molecular Cell 49(5):773-782.

[15] Naughton C, Avlonitis N, Corless S, Prendergast JG, Mati IK, Eijk PP, Cockroft SL, Bradley M, Ylstra B, and Gilbert N (2013) Transcription forms and remodels supercoiling domains unfolding large-scale chromatin structures. Nat Struct Mol Biol 20(3):387-395.

[16] Rovinskiy N, Agbleke AA, Chesnokova O, Pang Z, and Higgins NP (2012) Rates of Gyrase Supercoiling and Transcription Elongation Control Supercoil Density in a Bacterial Chromosome. PLoS Genet 8(8):e1002845.

[17] Postow L, Hardy CD, Arsuaga J, and Cozzarelli NR (2004) Topological domain structure of the Escherichia coli chromosome. Genes Dev 18(14):1766-1779.

[18] Wang W, Li GW, Chen C, Xie XS, and Zhuang X (2012) Chromosome Organization by a Nucleoid-Associated Protein in Live Bacteria. Science 333: 1445-1449.

[19] Leng F, Chen B, and Dunlap DD (2011) Dividing a supercoiled DNA molecule into two independent topological domains. Proc. Natl. Acad Sci USA. 108(50):19973-19978.

[20] Rippe K (2001) Making contacts on a nucleic acid polymer. Trends in Biochemical Science 26(12):733-740.

[21] Norregaard K, Anderssona M, Sneppena K, Nielsenc PE, Brownd S, and Oddershedea LB (2013) DNA supercoiling enhances cooperativity and efficiency of an epigenetic switch. Proc. Natl. Acad Sci USA. 110(43): 17386–17391.

[22] Simmons RM, Finer JT, Chu S, and Spudich JA (1996) Quantitative measurements of force and displacement using an optical trap. Biophys J 70(4): 1813-1822.

[23] Strick TR, Allemand JF, Bensimon D, Bensimon A, and Croquette V (1996) The elasticity of a single supercoiled DNA molecule. Science 271(5257):1835-1837.

[24] Florin EL, Moy VT and Gaub HE (1994) Adhesion Forces between Individual Ligand-Receptor Pairs. Science 264(5157): 415-417.

[25] Vilfan ID, Lipfert J, Koster DA, Lemay SG, and Dekker NH (2009) Magnetic Tweezers for Single-Molecule Experiments. Chapter 13, Handbook of Single-Molecule Biophysics, Springer.

[26] Pincet F and Husson J (2005) The solution to the streptavidin–biotin paradox: The influence of history on the strength of single molecular bonds. Biophys J 89: 4374–4381.

[27] Merkel R, Nassoy P, Leung A, Ritchie K, and Evans E (1999) Energy landscapes of receptor–ligand bonds explored with dynamic force spectroscopy. Nature 397: 50–53.

[28] Dammer U, Hegner M, Anselmetti D, Wagner P, Dreier M, Huber W, and Güntherodt HJ (1996) Specific antigen/antibody interactions measured by force microscopy. Biophy J 70: 2437–2441;

[29] Moy VT, Florin EL, and Gaub HE (1994) Intermolecular forces and energies between ligands and receptors. Science 266: 257–259.

[30] Lee GU, Kidwell DA, and Colton RJ (1994) Sensing discrete streptavidin–biotin interactions with atomic-force microscopy. Langmuir 10: 354–357.

[31] Wang MD, Schnitzer MJ, Yin H, Landick R, Gelles J, Block SM (1998) Force and velocity measured for single molecules of RNA polymerase. Science 282(5390): 902-907.

[32] Bockelmann U, Thomen P, Essevaz-Roulet B, Viasnoff V, Heslot F (2002) Unzipping DNA with optical tweezers: high sequence sensitivity and force flips. Biophys J 82(3): 1537-1553.

[33] Smith DE, Tans SJ, Smith SB, Grimes S, Anderson DL, Bustamante C (2001) The bacteriophage phi 29 portal motor can package DNA against a large internal force. Nature 413(6857): 748-752.

[34] Ma J, Bai L, and Wang MD (2013) Transcription Under Torsion. Science 340(6140):1580-1583.

[35] Smith SB, Finzi L, and Bustamante C (1992) Direct Mechanical Measurements of the Elasticity of Single DNA-Molecules by Using Magnetic Beads. Science 258(5085): 1122-1126.

[36] Strick TR, Croquette V, and Bensimon D (1998) Homologous pairing in stretched supercoiled DNA. Proc. Natl. Acad Sci USA. 95(18): 10579-10583.

[37] Tempestini A, Cassina V, Brogioli D, Ziano R, Erba S, Giovannoni R, Cerrito MG, Salerno D, Mantegazza F (2013) Magnetic tweezers measurements of the nanomechanical stability of DNA against denaturation at various conditions of pH and ionic strength. Nucleic Acids Res. 41(3): 2009–2019.

[38] Purohit PK (2010) Shape and energetics of DNA plectonemes. IUTAM symposium on Cell, Molecular and Tissue.

[39] Clauvelin N, Audoly B, and Neukirch S (2009) Elasticity and Electrostatics of Plectonemic DNA. Biophys J 96(9): 3716-3723.

[40] Moroz JD and Nelson P (1998) Entropic elasticity of twist-storing polymers. Macromolecules 31(18): 6333-6347.

[41] Marko JF (2007) Torque and dynamics of linking number relaxation in stretched supercoiled DNA. Physical Review E 76(2), 021926.

[42] Marko JF and Siggia ED (1995) Stretching DNA. Macromolecules 28(26): 8759-8770.

[43] Mosconi F, Allemand JF, Bensimon D, and Croquette V (2009) Measurement of the Torque on a Single Stretched and Twisted DNA Using Magnetic Tweezers. Physical Review Letters 102(7), 078301.

[44] Bednar J, Furrer P, Katritch V, Stasiak AZ, Dubochet J, and Stasiak A (1995) Determination of DNA Persistence Length by Cryoelectron Microscopy - Separation of the Static and Dynamic Contributions to the Apparent Persistence Length of DNA. J Mol Biol 254(4): 579-591.

[45] Bustamante C, Marko JF, Siggia ED, and Smith S (1994) Entropic elasticity of lambda-phage DNA. Science 265: 1599–1600.

[46] Bouchiat C, Wang MD, Allemand J, Strick T, Block SM, and Croquette V (1999) Estimating the persistence length of a worm-like chain molecule from force-extension measurements. Biophys J 76: 409–413.

[47] Vologodskii A (1994) DNA extension under the action of an external force. Macromolecules 27: 5623–5625.

[48] Shao Q. (2011) DNA elasticity and effects on Type II topoisomerases. PhD Dissertation, Emory University.

[49] Sarkar A, Leger JF, Chatenay D, and Marko JF (2001) Structural transitions in DNA driven by external force and torque. Phys Rev E Stat Nonlin Soft Matter Phys 63: 051903.

[50] Gao N, Shearwin K, Mack J, Finzi L, and Dunlap D (2013) Purification of bacteriophage lambda repressor. Protein Expression and Purification 91(1): 30-36.

[51] Manzo C and Finzi L (2010) Quantitative Analysis of DNA-Looping Kinetics from Tethered Particle Motion Experiments. Methods In Enzymology, ed Nils GW (Academic Press), Volume 475, pp 199-220.

[52] Watkins LP and Yang H (2005) Detection of Intensity Change Points in Time-Resolved Single-Molecule Measurements. J. Phys. Chem. B 109(1): 617-628.

[53] Leger JF, Romano G, Sarkar A, Robert J, Bourdieu L, Chatenay D, and Marko JF (1999) Structural transitions of a twisted and stretched DNA molecule. Physical Review Letters 83(5): 1066-1069.

[54] van Loenhout MTJ, de Grunt MV, and Dekker C (2012) Dynamics of DNA Supercoils. Science. 338(6103): 94-97.

[55] Bryant Z, Stone MD, Gore J, Smith SB, Cozzarelli NR, and Bustamante C (2003) Structural transitions and elasticity from torque measurements on DNA. Nature 424(6946): 338-341.

[56] Celedon A, Wirtz D, and Sun S (2010) Torsional mechanics of DNA are regulated by small molecule intercalation. J Phys Chem B 114(50): 16929-16935.

[57] Strick TR, Bensimon D, and Croquette V (1999) Micro-mechanical measurement of the torsional modulus of DNA. Genetica 106(1-2): 57-62.

[58] Mazur AK (2010) Anharmonic Torsional Stiffness of DNA Revealed under Small External Torques. Physical Review Letters 105(1): 018102.

[59] Spakowitz AJ (2006) Wormlike chain statistics with twist and fixed ends. EPL (Europhysics Letters) 73(5): 684.

[60] Fujimoto BS, Brewood GP, and Schurr JM (2006) Torsional rigidities of weakly strained DNAs. Biophys J 91(11): 4166-4179.

[61] Hagerman PJ (1988) Flexibility of DNA. Annual Review of Biophysics and Biophysical Chemistry 17(1): 265-286.

[62] Vlijm R, Smitshuijzen JS, Lusser A, and Dekker C (2012) NAP1-assisted nucleosome assembly on DNA measured in real time by single-molecule magnetic tweezers. PLoS ONE 7(9): e46306.

[63] Lipfert J, Klijnhout S, and Dekker NH (2010) Torsional sensing of small-molecule binding using magnetic tweezers. Nucleic Acids Res 38(20): 7122-32.

[64] Hensel Z, Weng X, Lagda AC, and Xiao J (2013) Transcription-factor-mediated DNA looping probed by high-resolution, single-molecule imaging in live *E. coli* cells. PLoS Biol 11(6): e1001591.

[65] Saiz L and Vilar JMG (2006) DNA looping: the consequences and its control. Current Opinion in Structural Biology 16(3): 344-350.

[66] Galburt EA, Grill SW, Wiedmann A, Lubkowska L, Choy J, Nogales E, Kashlev M, and Bustamante C (2007) Backtracking determines the force sensitivity of RNAP II in a factor-dependent manner. Nature 446(7137): 820-823.

[67] Leng F, Amado L, and McMacken R (2004) Coupling DNA Supercoiling to Transcription in Defined Protein Systems. Journal Of Biological Chemistry 279(46): 47564-47571.

[68] Niehus E, Cheng E, and Tan M (2008) DNA supercoiling-dependent gene regulation in Chlamydia. J Bacteriol 190(19): 6419-6427.

[69] Wang H and Benham CJ (2008) Superhelical destabilization in regulatory regions of stress response genes. PLoS Comput Biol 4(1): e17.

[70] Ye F, Brauer T, Niehus E, Drlica K, Josenhans C, Suerbaum S (2007) Flagellar and global gene regulation in Helicobacter pylori modulated by changes in DNA supercoiling. International Journal of Medical Microbiology 297(2): 65-81.

[71] Sobetzko P, Travers A, and Muskhelishvili G (2012) Gene order and chromosome dynamics coordinate spatiotemporal gene expression during the bacterial growth cycle. Proc. Natl. Acad Sci USA. 109(2): E42–E50.

[72] Planas-Paz L, Strilic´ B, Goedecke A, Breier G, Fässler R, and Lammert E. (2012) Mechanoinduction of lymph vessel expansion. EMBO J 31: 788-804.

[73] Dupont S, Morsut L, Aragona M, Enzo E, Giulitti S, Cordenonsi M, Zanconato F, Le Digabel J, Forcato M, Bicciato S, Elvassore N, and Piccolo S (2011) Role of YAP/TAZ in mechanotransduction. Nature 2011, 474: 179-183.

[74] Guilluy C, Swaminathan V, Garcia-Mata R, O'Brien ET, Superfine R, and Burridge K (2011) The Rho GEFs LARG and GEF-H1 regulate the mechanical response to force on integrins. Nat Cell Biol 13: 722-727.

[75] Ehrlicher AJ, Nakamura F, Hartwig JH, Weitz DA, and Stossel TP (2011) Mechanical strain in actin networks regulates FilGAP and integrin binding to filamin A. Nature 478: 260-263.

[76] Ingber DE (2006) Cellular mechanotransduction: putting all the pieces together again. FASEB J 20(7): 811-27.

[77] del Rio A, Perez-Jimenez R, Liu R, Roca-Cusachs P, Fernandez JM, and Sheetz MP (2009) Stretching single talin rod molecules activates vinculin binding. Science 323: 638-641.

[78] Margadant F, Chew LL, Hu X, Yu H, Bate N, Zhang X, and Sheetz M (2011) Mechanotransduction in vivo by repeated talin stretch-relaxation events depends upon vinculin. PLoS Biol 9:e1001223.

[79] Chen W, Lou J, Evans EA, and Zhu C (2012) Observing force-regulated conformational changes and ligand dissociation from a single integrin on cells. J Cell Biol 199: 497-512.

[80] Grashoff C, Hoffman BD, Brenner MD, Zhou R, Parsons M, Yang MT, McLean MA, Sligar SG, Chen CS, Ha T, and Schwartz MA (2010) Measuring mechanical tension across vinculin reveals regulation of focal adhesion dynamics. Nature 466: 263–266.

[81] Legant WR, Miller JS, Blakely BL, Cohen DM, Genin GM, and Chen CS (2010) Measurement of mechanical tractions exerted by cells in three-dimensional matrices. Nature Methods 7: 969–971.

[82] Wang X and Ha T (2013) Defining Single Molecular Forces Required to Activate Integrin and Notch Signaling. Science 340: 991–994.

[83] Campàs O, Mammoto T, Hasso S, Sperling RA, O'Connell D, Bischof AG, Maas R, Weitz DA, Mahadevan L, and Ingber DE (2014) Quantifying cell-generated mechanical forces within living embryonic tissues. Nature Methods 11: 183–189.

[84] Stabley DR, Jurchenko C, Marshall SS, and Salaita KS (2012) Visualizing Mechanical Tension across Membrane Receptors with a Fluorescent Sensor. Nature Methods 9: 64–67.

[85] Liu Y, Yehl K, Narui Y, and Salaita K (2013) Tension Sensing Nanoparticles for Mechano-imaging at the Living Non-living Interface. J Am Chem Soc 135 (14): 5320–5323.

[86] Neuman KC and Nagy A (2008) Single-molecule force spectroscopy: optical tweezers, magnetic tweezers and atomic force microscopy. Nat Methods. 5(6): 491-505.

[87] Shroff H, Reinhard BM, Siu M, Agarwal H, Spakowitz A, and Liphardt J (2005) Biocompatible Force Sensor with Optical Readout and Dimensions of 6 nm^3. Nano Lett. 5(7): 1509-1514.

[88] Brutzer H, Schwarz FW, and Seidel R (2012) Scanning Evanescent Fields Using a pointlike Light Source and a Nanomechanical DNA Gear. Nano Lett. 12: 473−478.

[89] Graham JS, Johnson RC, and Marko JF (2011) Concentration-dependent exchange accelerates turnover of proteins bound to double-stranded DNA. Nucleic Acids Res. 39(6): 2249–2259.

[90] Lee M, Kim SH, and Hong SC (2010) Minute negative superhelicity is sufficient to induce the B-Z transition in the presence of low tension. Proc. Natl. Acad Sci USA. 107(11) : 4985–4990.

[91] Long X, Parks JW, Bagshaw CR, and Stone MD (2013) Mechanical unfolding of human telomere G-quadruplex DNA probed by integrated fluorescence and magnetic tweezers spectroscopy. Nucleic Acids Res. 41(4) : 2746–2755.

[92] Aitken CE, Marshall RA, and Puglisi JD (2008) An Oxygen Scavenging System for Improvement of Dye Stability in Single-Molecule Fluorescence Experiments. Biophys J 94: 1826–1835.

[93] Pang Z, Laplante NE, and Filkins RJ (2012) Dark pixel intensity determination and its applications in normalizing different exposure time and autofluorescence removal. J Microscopy 246(1) : 1-10.

[94] Woodside MT, Behnke-Parks WM, Larizadeh K, Travers K, Herschlag D, and Block SM (2006) Nanomechanical measurements of the sequence-dependent folding landscapes of single nucleic acid hairpins. Proc Natl Acad Sci USA. 103: 6190-6195.

[95] Janissen R, Oberbarnscheidt L, and Oesterhelt F (2009) Optimized straight forward procedure for covalent surface immobilization of different biomolecules for single molecule applications. Colloids and Surfaces B: Biointerfaces 71, 200–207.

Appendix 1 DNA-Nicking Gel Assay

All the work listed here in the Appendix 1 was done by our collaborators Geraldine Fulcrand and Fenfei Leng from Florida International University. This section is adapted from part of a submitted manuscript for future publication (Ding et al., under revision).

Materials and Methods

1) Analysis of supercoils constrained by cI-mediated looping of plasmids

1 mM DTT was assembled on ice and incubated for 30 min at 37 ºC, before nicking a mixture (320μl) containing 0.156 nM of negatively supercoiled DNA template and 170 nM or various concentrations of wild-type λ repressor (cI) in a buffer consisting of 20 mM Tris-acetate (pH 7.9 at 25 ºC), 50 mM potassium acetate, and 10 mM magnesium acetate. The supercoiled DNA templates were then digested by 20 units of Nb.BbvCI at 37 ºC for 2 min or as indicated. Next, a large excess of a double-stranded oligonucleotides containing the Nb.BbvCI recognition site was added to the reaction mixtures to inhibit further plasmid digestion. The nicked DNA templates were ligated using T4 DNA ligase in the presence of 1 mM ATP at 37 ºC for 5 min, and the reaction was terminated by extraction with an equal volume of phenol. Plasmids were precipitated in ethanol and dissolved in 25 μL of 10 mM Tris-HCl buffer (pH 8.5). The ligated DNA products were separated using 1% agarose gel electrophoresis in the absence or presence of 1 μg/mL of chloroquine and the linking numbers of the topoisomers were calculated from the gel images stained with ethidium bromide using KODAK 1D Image Analysis Software.

2) Determining the superhelical density of supercoiled plasmids before CI addition

100 µl mixtures containing 1.5 µg of negatively supercoiled DNA template, 200 nM of E.coli DNA topoisomerase I, and various concentrations of ethidium bromide in 20 mM Tris-acetate (pH 7.9 at 25 ºC), 50 mM potassium acetate, 10 mM magnesium acetate, 1 mM DTT, 10 µg/mL BSA were assembled on ice and incubated for 15 min at 37 ºC. The reactions were terminated by extraction with an equal volume of phenol. The DNA topoisomers were isolated and subjected to 1% agarose gel electrophoresis in the absence or presence of 0.5, 1, or 2.5 µg/mL of chloroquine for the determination of the supercoiling density (S1).

Results

Lambda repressor-secures DNA loops and is a barrier to supercoil diffusion

It was previously demonstrated using gel electrophoresis of topoisomers that soluble proteins like the Lac and Gal repressors and the λ O protein can trap supercoils in DNA loops and form barriers to prevent supercoil diffusion between topological domains (18). One experiment used DNA-binding proteins that recognize and simultaneously bind widely separated sequences to partition plasmids into topologically distinct segments before nicking one segment with a site-specific endonuclease for various time intervals before re-ligation, and characterizing the resulting topoisomers. This method was adopted (Figure S1) to test whether and to what extent lambda repressor trapped supercoils in the larger of the two segments it created in pDL1051 or pDL2317 plasmids, and how rapidly

torsion traverses the lambda repressor barrier from that segment into the smaller, nicked segment where it dissipates. Nicking has been shown to relieve torsion on the time scale of milliseconds (S2).

The lambda repressor efficiently trapped supercoils in both plasmids with initial supercoiling densities around -6.1% (Figure S2) that decayed exponentially over time in an apparently stochastic, single-step process (Figure S3, Table S1). Torsion dissipated through the cI oligomer more slowly in pDL1051 than in pDL2317. The exponential decay constant for the disappearance of supercoiling from the plasmid was 7.6 minutes for the 1051 bp loop versus 1.8 minutes for the 2317 bp loop. All of the loops created by lambda repressor in these plasmids are long enough so that any strain due to bending DNA was negligible, and the supercoiling energies present in the initially supercoiled, 4000 bp segments were similar. This result suggests that the entropy change associated with looping governs the stability of the barrier; which is smallest for loops of approximately 400 bp and increasingly penalizes the formation of progressively longer loops, governs the stability of the barrier. The higher entropic penalty associated with securing a 2317 loop would make it less stable than the 1051 bp loop.

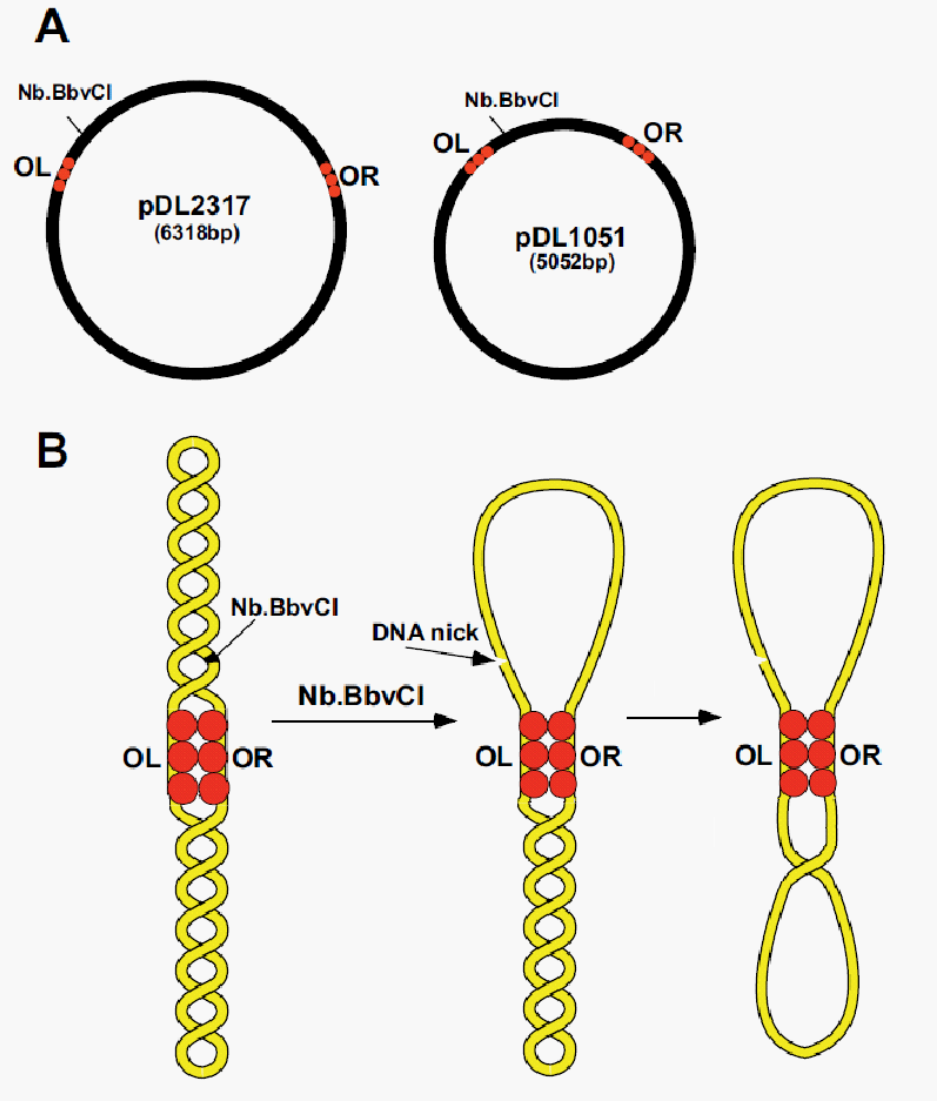

Figure S1. Schematic representation of the DNA-nicking gel assay. (A) The location of a restriction site for the enzyme Nb.BbvCI is shown relative to enterobacteria phage lambda *OR* and *OL* operators in plasmids pDL2317 and pDL1051. Red dots represent lambda operators *OL1*, *OL2*, *OL3*, *OR1*, *OR2*, and *OR3*. (B) A topological barrier model for lambda cI repressor. Upon binding to *OL* and *OR* operators, the DNA-looping protein lambda cI repressor (red circles) functions as a barrier that blocks supercoil diffusion. A DNA nick introduced by the endonuclease Nb.BbvCI quickly relaxes superhelicity within the upper loop. Superhelicity in the bottom loop slowly escapes through the cI-mediated topological barrier where dissipates quickly as well.

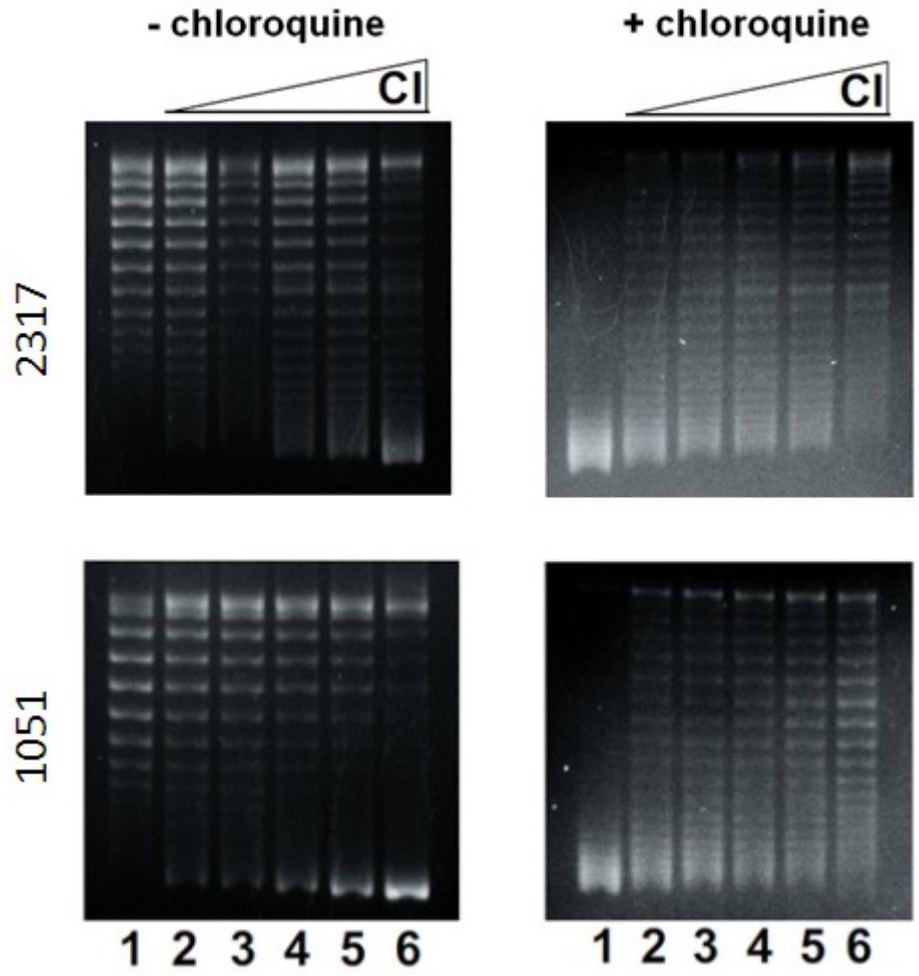

Figure S2. Protein-divided topological domains in plasmids. Lambda repressor (cI) divided supercoiled plasmids into two independent topological domains. The DNA-nicking assays were performed as described under Materials and Methods. In addition to 0.156 nM of either pDL1051 or pDL2317, the reaction mixtures also contained 0, 10, 20, 52, 80, or 170 nM λ cI (lanes 1-6 respectively) and Nb.BbvCI (20 units). The DNA molecules (topoisomers) were isolated and subjected to agarose gel electrophoresis in absence (-) or presence (+) of 2.5 μg/mL chloroquine. Leftmost lanes (1) contains DNA relaxed at 37 °C and slightly (+) supercoiled because the gels were run at 24 °C.

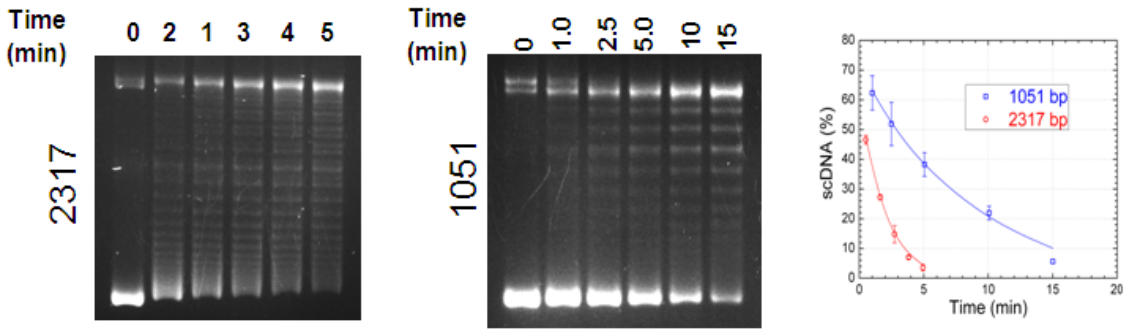

Figure S3. Supercoiling dissipation through the protein-binding junction. Supercoiling slowly dissipated over several minutes from the larger 4000 bp domain of plasmids partitioned by a loop mediated by 170 nM cI. DNA-nicking assays were performed as described under Materials and Methods with incubation at 37 °C. At the indicated times, the DNA was isolated and subjected to agarose gel electrophoresis without chloroquine (left, pDL2317; middle, pDL1051). The percentage of remaining supercoiled DNA was plotted as a function of the incubation time (right). Fitting with a single exponential decay yielded a decay constant of 7.6 or 1.8 min for loops of 1051 or 2317 bp, respectively.

Plasmid	Nicked segment length (bp)[a]	Supercoil density (s)[b]	$t_{1/2}$ (min)[c]	Supercoils constrained in loop[d]
pDL1051	1051	-0.061	10.41 ± 0.29	7.56 ± 0.59
pDL2317	2317	-0.062	2.44 ± 0.42	11.94 ± 0.45

Table S1. Data on supercoiling diffusion in different plasmids. The diffusion of superhelicity within plasmids from cI-secured loops into the nicked adjoining segment. [a] The nicked segment is the shorter separation between the lambda OL and OR operators. [b] The DNA superhelical densities of plasmids pDL1051 and pDL2317 were determined as described in Materials and Methods. [c] $t_{1/2}$ represents the decay constant of supercoiling, determined by the DNA-nicking method as described in Material and Methods. [d] Values refer to supercoils constrained in the DNA-loops of plasmids pDL1051 and pDL2317 before nicking, which were calculated based on data shown in Figure S3.

Additional references

[S1] Clark DJ and Leblanc B (2009) Analysis of DNA supercoiling induced by DNA-protein interactions. Methods Mol Biol 543:523-535.

[S2] Crut A, Koster DA, Seidel R, Wiggins CH, and Dekker NH (2007) Fast dynamics of supercoiled DNA revealed by single-molecule experiments. Proc. Natl. Acad Sci USA. 104(29):11957-11962.